

Temperature inhomogeneities cause the abundance discrepancy in H II regions

J. Eduardo Méndez-Delgado^{1*}, César Esteban^{2,3}, Jorge García-Rojas^{2,3}, Kathryn Kreckel¹ and Manuel Peimbert⁴

^{1*}Astronomisches Rechen-Institut, Zentrum für Astronomie der Universität Heidelberg, Mönchhofstraße 12-14, Heidelberg, D-69120, Baden-Württemberg, Germany.

²Instituto de Astrofísica de Canarias, (IAC), Vía Láctea, 1, San Cristóbal de La Laguna, E-38205, Santa Cruz de Tenerife, Spain.

³Departamento de Astrofísica, Universidad de La Laguna, Astrofísico Francisco Sánchez, s/n., San Cristóbal de La Laguna, E-38206, Santa Cruz de Tenerife, Spain.

⁴Instituto de Astronomía, Universidad Nacional Autónoma de México, Apartado Postal 70-264, Coyoacán, 04510, Mexico City, México.

*Corresponding author(s). E-mail(s): jemd@uni-heidelberg.de;

Abstract

H II regions, ionized nebulae where massive star formation has taken place, exhibit a wealth of emission lines that are the fundamental basis for estimating the chemical composition of the Universe. For more than 80 years, a discrepancy of at least a factor of two between heavy-element abundances derived with collisional excited lines (CELs) and the weaker recombination lines (RLs) has thrown our absolute abundance determinations into doubt. Heavy elements regulate the cooling of the interstellar gas, being essential to the understanding of several phenomena such as nucleosynthesis, star formation and chemical evolution. In this work, we use the best available deep optical spectra of ionized nebulae to analyze the cause of this abundance discrepancy problem. We find for the first time general observational evidence in favor of the temperature inhomogeneities within the gas, quantified by t^2 . The temperature inhomogeneities inside H II regions are affecting only the gas of high ionization degree and producing the abundance discrepancy problem. This

work implies that the metallicity determinations based on CELs must be revised, as they can be severely underestimated, especially in the regions of lower metallicity, such as the JWST high- z galaxies. We present methods to estimate these corrections, which will be critical for robust interpretations of the chemical composition of the Universe over cosmic time.

Keywords: H II regions, Interstellar abundances, Galaxy abundances, Galaxy chemical evolution

Since the pioneering work by [1], in essentially all studies where the weak recombination lines (RLs) of heavy-element ions have been detected in ionized nebulae, they imply systematically higher heavy element abundances than those derived from the stronger collisionally excited lines (CELs). Given that the line emission is produced by the same ion through different mechanisms, the abundance discrepancy points to inconsistencies or missing physics in the assumptions underlying the derivation of chemical abundances. Several hypotheses have been proposed over the last 80 years in attempts to resolve this issue. For instance, temperature inhomogeneities [2], chemical inhomogeneities [3], errors in the atomic recombination coefficients [4], a non-Maxwellian electron velocity distribution [5], recombination contributions to the auroral CELs [6] and some others [7, 8]. The lack of clear observational confirmation of any of these ideas has prevented a general solution to this problem until now.

In H II regions the highly ionized gas is usually concentrated in the volume closest to the massive O or early B type stars, while the less ionized ions are concentrated in outer shells. Therefore, it is common to estimate a representative temperature for each volume of gas using CEL intensity ratios, usually $T_e([\text{O III}] \lambda 4363/\lambda 5007)$ and $T_e([\text{N II}] \lambda 5755/\lambda 6584)$ for the volume with high and low degree of ionization, respectively. The reason why the existence of temperature inhomogeneities within a given ionization zone can produce the abundance discrepancy is that the emission of CELs increases exponentially with temperature, whereas the emissivity of RLs depends on this parameter to a much lesser extent (decreasing proportionally to a power of T_e close to 1). Therefore, in case of inhomogeneities, T_e derived from CEL intensity ratios will be systematically biased towards higher values than the average temperature [2]. Then, by deriving the chemical composition based on the intensity ratio of CELs and H I RLs, an exponential systematic error towards lower abundances will be introduced. On the other hand, the intensity ratio of RLs is less sensitive to temperature, making it more suitable for deriving the true chemical composition of the gas. In the paradigm proposed by [2, 9], for a given ion X^{i+} , the average temperature of the gas will be:

$$T_0(X^{i+}) = \frac{\int T_e n_e n(X^{i+}) dV}{\int n_e n(X^{i+}) dV}, \quad (1)$$

where T_e , n_e are the electron temperature and density at a given volume of the nebula, whereas $n(X^{i+})$ is the particle density of the ion. If there are temperature inhomogeneities, these can be quantified by the root mean square deviation from the averaged temperature:

$$t^2(X^{i+}) = \frac{\int [T_e - T_0(X^{i+})]^2 n_e n(X^{i+}) dV}{T_0(X^{i+})^2 \int n_e n(X^{i+}) dV}. \quad (2)$$

We use a collection of 20 and 23 deep optical spectra of Galactic and extragalactic H II regions, respectively as well as 8 spectra of Galactic ring nebulae (RNe), which are nebulae created by mass-loss episodes from young very massive stars. These data have the best quality available in the literature, being carefully and homogeneously reduced and analyzed over more than 20 years by our research group, containing the following characteristics: (i) have at least one line detected from the recombination O II multiplet V1, free of line blending with other lines that are not O II V1 RLs or observational issues. (ii) uncertainties in the line ratios smaller than 40%. (iii) reliable detections of both temperature-sensitive [N II] $\lambda 5755$ and [O III] $\lambda 4363$ CELs. Following the so-called direct method, we calculate the electron density of the nebulae, as well as $T_e([\text{O III}] \lambda 4363/\lambda 5007)$, $T_e([\text{N II}] \lambda 5755/\lambda 6584)$ and $T_e([\text{Ar III}] \lambda 5192/\lambda 7751)$ when available. We derive $T_e(\text{O II V1}/[\text{O III}] \lambda 5007)$ using the formalism proposed by [10] with the updated atomic data from [11].

Not surprisingly, in all cases, O^{2+}/H^+ derived from the O II V1 RLs is found to be higher than the same ratio derived from the [O III] $\lambda 5007$ CEL (see Table A8). The ratio of both ionic abundances is called the abundance discrepancy factor (ADF). By comparing the $T_e([\text{O III}] \lambda 4363/\lambda 5007)$ and $T_e(\text{O II V1}/[\text{O III}] \lambda 5007)$ -determined using Eqs. 10 and 11 from [10]-, we derive $T_0(\text{O}^{2+})$ and $t^2(\text{O}^{2+})$. The last parameter is the degree of spatial temperature variations within the high ionization zone that is required in order to reconcile the O^{2+}/H^+ ratios derived from RLs and CELs.

Since the observations of the extragalactic H II regions cover the complete temperature structure, we will initially focus our analysis on these regions in order to avoid the scatter that may be induced by aperture effects. Contrary to what was argued in several studies [7, 12, 13] that were limited to a small number of H II regions, there is no “typical” $t^2(\text{O}^{2+})$ value for these nebulae (See Table A7). As pointed out by [14–16], very high values of $t^2(\text{O}^{2+})$ can be found in “low metallicity” H II regions. However, the connection between $t^2(\text{O}^{2+})$ and the physical conditions of the gas was not obvious in these previous studies. In Fig. 1 we show the missing connection, $t^2(\text{O}^{2+})$ is linearly correlated with $\Delta T_e = T_e([\text{O III}] \lambda 4363/\lambda 5007) - T_e([\text{N II}] \lambda 5755/\lambda 6584)$, as follows:

$$t^2(\text{O}^{2+}) = (2.90 \pm 0.21) \times 10^{-5} \Delta T_e + (4.68 \pm 0.18) \times 10^{-2} (\text{K}). \quad (3)$$

The explanation and the implications of this correlation are the following:

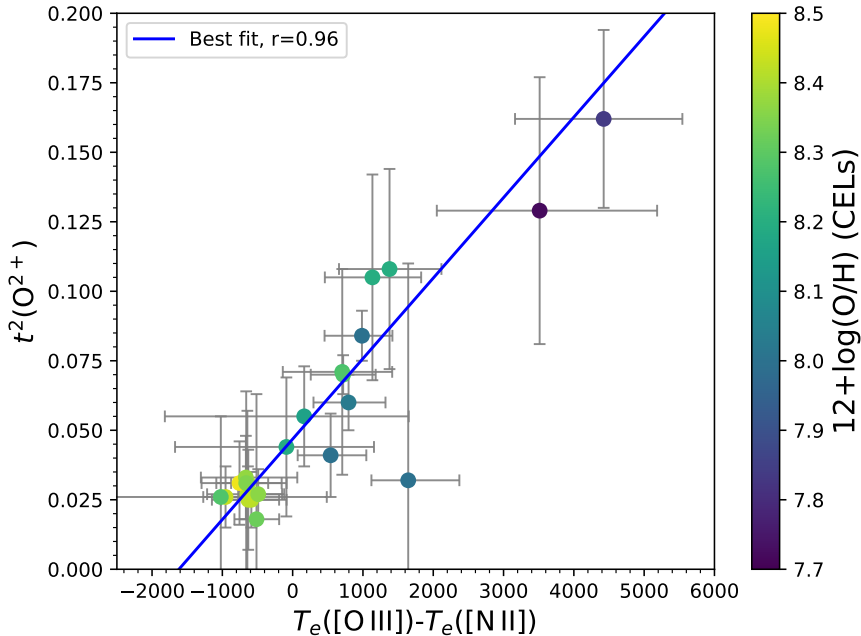


Fig. 1 Linear correlation between $t^2(\text{O}^{2+})$, the temperature inhomogeneities parameter value required to solve the abundance discrepancy problem and the difference of the derived temperatures of the ionized gas for extragalactic H II regions. The color bar corresponds to the O/H abundance derived from CELs assuming a homogeneous temperature structure ($t^2 = 0$). The Pearson correlation coefficient of the fit (r) is 0.96.

- The linear relationship between $t^2(\text{O}^{2+})$ and ΔT_e is a consequence of the fact that $T_e([\text{N II}] \lambda 5755/\lambda 6584)$ behaves as the average temperature in the N^+ volume (See Eq. (2)). This implies that temperature inhomogeneities are negligible in the low ionization zone (i.e. $t^2(\text{O}^+) \approx 0$). This is demonstrated in Fig. 2, where a tight linear correlation between $T_e([\text{N II}] \lambda 5755/\lambda 6584)$ and $T_0(\text{O}^{2+})$ is presented.
- The fact that $T_e(\text{O II V1}/[\text{O III}] \lambda 5007)$ (practically identical to $T_0(\text{O}^{2+})$ in H II regions) is correlated with $T_e([\text{N II}] \lambda 5755/\lambda 6584)$ also demonstrates that the first value is physically representing a gas temperature.
- As $T_e(\text{O II V1}/[\text{O III}] \lambda 5007) < T_e([\text{O III}] \lambda 4363/\lambda 5007)$, with the first being a real value of temperature, we show that a physical process is acting preferentially in the inner high ionization volume, increasing the intensity of the temperature sensitive $[\text{O III}] \lambda 4363$ CEL. This demonstrate the existence of real temperature inhomogeneities.
- Therefore $t^2(\text{O}^{2+})$ is not an ad-hoc parameter to solve the abundance discrepancy of the O^{2+} ion, it is indeed describing inhomogeneities in the temperature of the highly ionized gas.

On the first point mentioned above, it should be noted that $T_e([\text{N II}]\lambda 5755/\lambda 6584)$ is not involved in the estimation of $T_0(\text{O}^{2+})$ or $T_e(\text{O II VI}/[\text{O III}]\lambda 5007)$ in any sense. We interpret the relationship shown in Fig. 2 as a consequence of the natural stratification of temperatures expected in the photoionized gas due to the combination of the hardening of the stellar radiation and the stronger cooling from $[\text{O III}]$ lines, which are more efficient at cooling than those of $[\text{O II}]$ [17, 18]. The linear fit between both quantities is presented in Eq. (4).

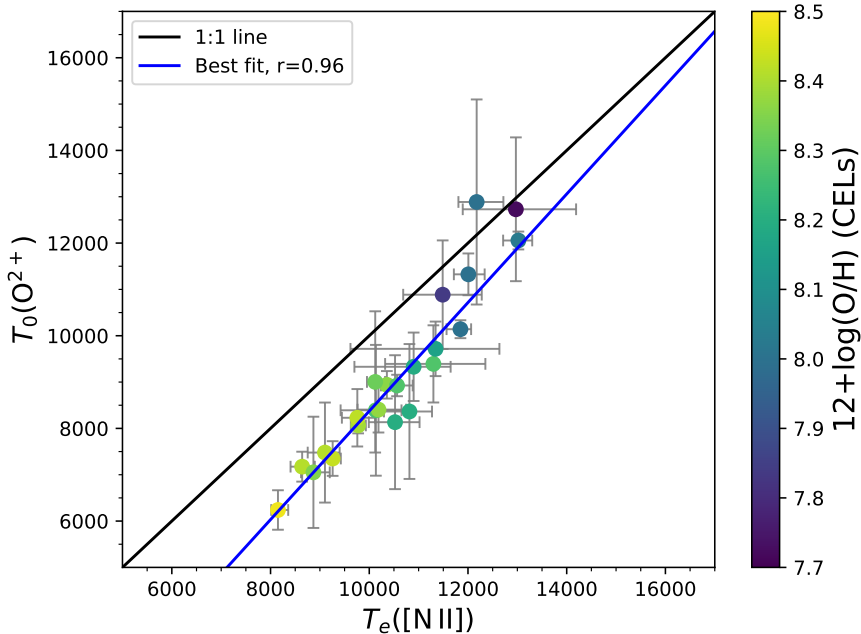


Fig. 2 Relation between $T_e([\text{N II}]\lambda 5755/\lambda 6584)$ and $T_0(\text{O}^{2+})$ for extragalactic H II regions.

$$T_0(\text{O}^{2+}) = (1.17 \pm 0.05) \times T_e([\text{N II}]) - (3340 \pm 470) \text{ (K)}. \quad (4)$$

When we extend the analysis to the Galactic H II regions and RNe, as shown in Fig. 3, we observe that in general they follow the same trend as the extragalactic H II regions. Five spectra from different areas of NGC 6888 [19], a bubble of ionized gas created by the Wolf-Rayet WN6 star WR136 and three from NGC 7635 [19], created by the O6.5(n)fp star BD+60 2522 [20] and the surrounding interstellar gas show also a good agreement with the general trend of the H II regions. This is remarkable in the case of some peripheral zones of NGC 6888, that show particularly large values of $t^2(\text{O}^{2+})$. This implies that stellar feedback processes can contribute to the inhomogeneous heating of the gas and are related to the origin of temperature inhomogeneities. This is

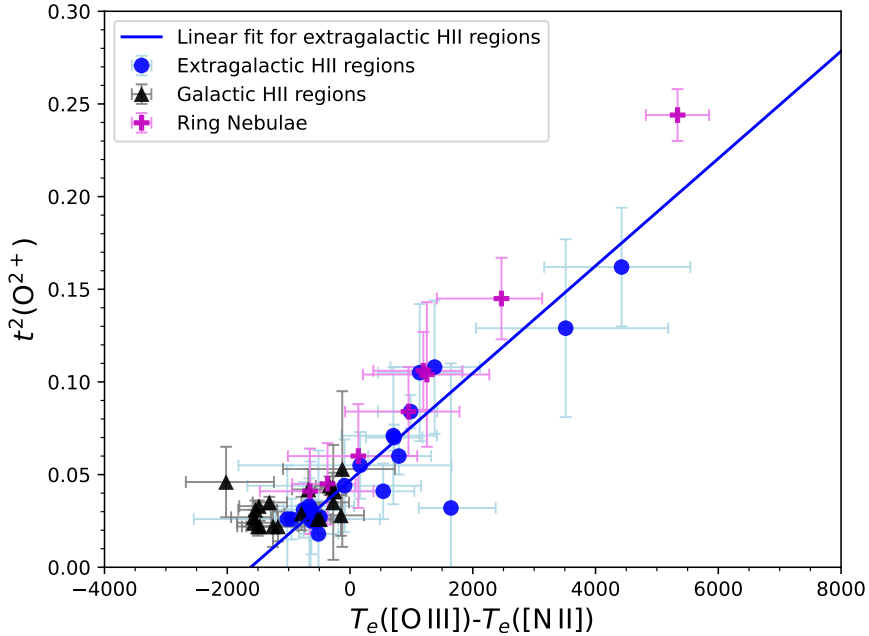


Fig. 3 $t^2(\text{O}^{2+})$ versus ΔT_e relation for Galactic and extragalactic H II regions and ring nebulae.

consistent with the fact that the gas with a high degree of ionization, which is located physically closer to the ionizing stars in typical H II regions, is the most affected one by the temperature inhomogeneities. Variations in the hardness of the stellar ionizing spectra may also contribute to $t^2(\text{O}^{2+})$ [21, 22].

To test the impact of our results on the metallicity of our sample of extragalactic H II regions, we compare the effect of considering $t^2 > 0$ only in the high ionization volume. The results are shown in Fig. 4, and highlight that the metallicity underestimation tends to be larger at lower metallicities, reaching values as high as 0.5 dex. Considering these results, we can infer a $T_e([\text{N II}])$ $\lambda 5755/\lambda 6584$ -metallicity relation, provided in Eq. (5) and shown in Fig. 5, which allows a quick estimation of the metallicity considering $t^2(\text{O}^{2+}) > 0$.

$$12 + \log(\text{O}/\text{H}) = (-1.19 \pm 0.14) \times 10^{-4} T_e([\text{N II}]) + (9.68 \pm 0.15) \text{ (K)}. \quad (5)$$

Based on deep optical spectra of Galactic and extragalactic H II regions and ring nebulae, we conclude that temperature inhomogeneities are present within these nebulae. These inhomogeneities cause the long-standing discrepancy between the heavy-element abundances determined with CELs and RLs. The observational evidence show that the temperature inhomogeneities affect only the volume of high degree of ionization, the closest to the ionizing stars.

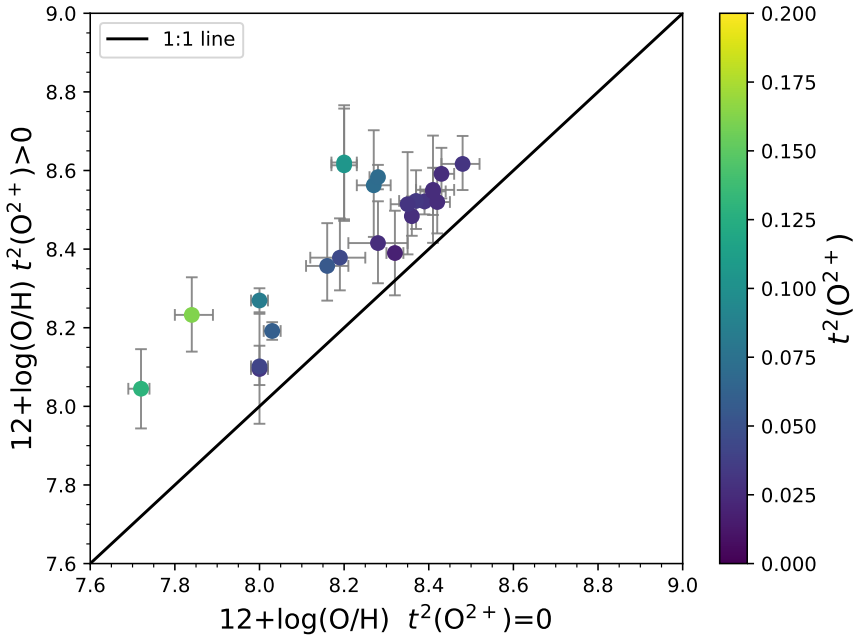


Fig. 4 Effects on metallicity of considering temperature inhomogeneities affecting only the high ionization volume in our sample of extragalactic H II regions.

This is a change of paradigm even for the community who consider $t^2 > 0$ in their studies. Stellar feedback processes and radiation hardness fluctuations of the stellar spectra are potential candidates to produce the observed inhomogeneities. The chemical abundances estimated with CELs, the most accessible observationally, must be revised because they are underestimated. Both the abundances determined by the direct method and those estimated by strong lines ones calibrated by observations require revision, since both depend on $T_e([\text{O III}] \lambda 4363/\lambda 5007)$. We provide Eq. (3), Eq. (4) and Eq. (5), which allow us to consider the effect of temperature inhomogeneities in the calculation of chemical abundances even if only CELs are observed. This is especially important in low metallicity H II regions where the values of $t^2(\text{O}^{2+})$ are higher, and metallicities are systematically underestimated (Fig. 4). This work has far-reaching implications for chemical evolution studies of galaxies, where the build-up of elements is treated as a cosmic clock. This is particular critical in our examination of the mass-metallicity relationships of galaxies [23], as well as recent efforts to directly track chemical evolution over cosmic time by using JWST to observe [O III] auroral lines in high- z galaxies [24–26]. Based on our findings, t^2 should be considered as a fundamental physical parameter both in observational and theoretical works.

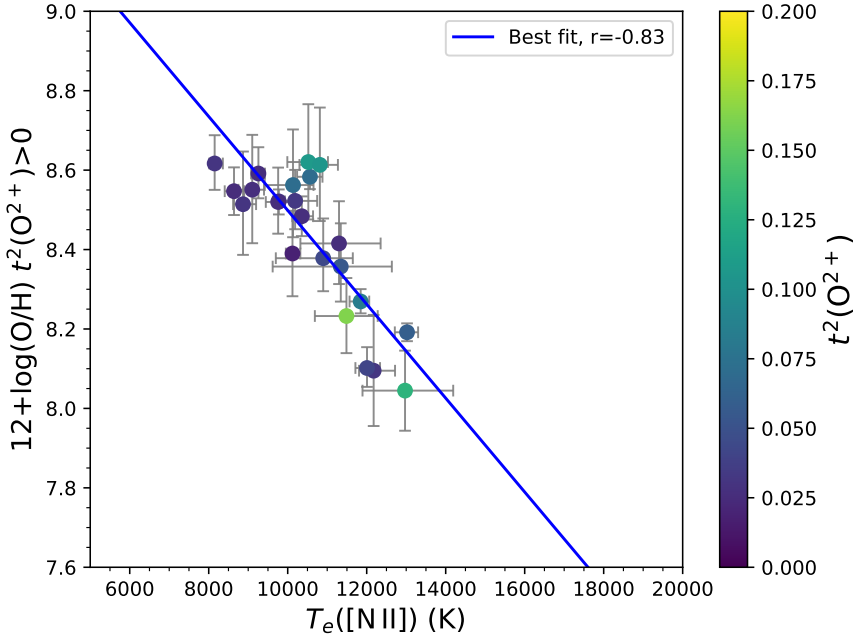


Fig. 5 $T_e(\text{[N II] } \lambda 5755/\lambda 6584)$ -metallicity relation considering $t^2(\text{O}^{2+}) > 0$ for our sample of extragalactic H II regions.

1 Methods

For the sample of nebulae presented in Tables A1, A2, A4 and A5, we derive the physical conditions and ionic abundances by the so-called direct method in a consistent way. All values obtained are based on the intensities reported in the reference spectra. We discard the use of lines with observational issues as telluric absorptions or sky line contaminations. We use PyNeb 1.1.13 [27] and the atomic data set provided in Table 1 to estimate the electron density (n_e) and temperature (T_e). As a first step, we derive the n_e - T_e cross-match convergence by solving the statistical equilibrium equations with the [S II] $\lambda 6731/\lambda 6716$, [O II] $\lambda 3726/\lambda 3729$, [Cl III] $\lambda 5538/\lambda 5518$, [Fe III] $\lambda 4658/\lambda 4702$ and [Ar IV] $\lambda 4740/\lambda 4711$ density diagnostics and the [O III] $\lambda 4363/\lambda 5007$, [N II] $\lambda 5755/\lambda 6584$, [Ar III] $\lambda 5192/\lambda 7135$ temperature diagnostics, using the task *getCrossTemDen* of PyNeb. For each density diagnostic, we average the convergence value of each cross-matching. Considering that [S II] $\lambda 6731/\lambda 6716$ and [O II] $\lambda 3726/\lambda 3729$ have their maximum sensitivity with density in the range of values $10^2 \text{ cm}^{-3} < n_e < 10^4 \text{ cm}^{-3}$ [28–31], whereas [Cl III] $\lambda 5538/\lambda 5518$, [Fe III] $\lambda 4658/\lambda 4702$ and [Ar IV] $\lambda 4740/\lambda 4711$ are good diagnostics in the range of $10^3 \text{ cm}^{-3} < n_e < 10^6 \text{ cm}^{-3}$ [32–37], we derive an average representative n_e adopting the following criteria:

- If $n_e(\text{[S II]}) < 100 \text{ cm}^{-3}$, we adopt $n_e < 100 \text{ cm}^{-3}$.

- If $100 \text{ cm}^{-3} < n_e([\text{S II}]) < 1000 \text{ cm}^{-3}$, we adopt the average value of $n_e([\text{S II}])$ and $n_e([\text{O II}])$.
- If $n_e([\text{S II}]) > 1000 \text{ cm}^{-3}$, we take the average values of $n_e([\text{S II}])$, $n_e([\text{O II}])$, $n_e([\text{Cl III}])$, $n_e([\text{Fe III}])$ and $n_e([\text{Ar IV}])$ when available.

In all cases, the averaged values are weighted by the inverse of the square of the error. All the extragalactic H II regions but one follow the first two criteria and therefore in Tables A1, A3 we only present $n_e([\text{O II}])$, $n_e([\text{S II}])$ as well as the adopted value. The exception is N 88A [38], where we follow the third criteria given its higher density. Therefore, in addition to the values of $n_e([\text{S II}])$ and $n_e([\text{O II}])$ shown in Table A1, we take into account $n_e([\text{Cl III}])=3890^{+280}_{-320} \text{ cm}^{-3}$, $n_e([\text{Ar IV}])=5860^{+910}_{-920} \text{ cm}^{-3}$ and $n_e([\text{Fe III}])=7570^{+3870}_{-2940} \text{ cm}^{-3}$ for N 88A. Once n_e is well established, we derive $T_e([\text{O III}] \lambda 4363/\lambda 5007)$, $T_e([\text{N II}] \lambda 5755/\lambda 6584)$ and $T_e([\text{Ar III}] \lambda 5192/\lambda 7751)$ when available, using the *getTemDen* task of PyNeb.

In the case of O II RLs, we consider only those from the multiplet V1, individually measured or blended with other lines of the same multiplet. In each region we sum the intensity of all the O II V1 observed lines and we estimate the intensity of the complete multiplet with the effective recombination coefficients from [11], which consider the population of the O II levels. These values of the total intensity of multiplet V1 are presented in the fifth column of the Table A7. The number of observed O II V1 lines is presented in the sixth column. Note that the relative intensity of the O II V1 RLs is independent of the temperature, while it depends on the density for values between $10^{2.5} \text{ cm}^{-3} < n_e < 10^4 \text{ cm}^{-3}$ [11]. Since the total intensity of the multiplet V1 is independent of the density, this could introduce some errors in high-density regions with an incorrect estimation of n_e (by an order of magnitude) and when only one O II V1 RL is detected. However, this case does not occur in our sample and our conclusions do not depend on this.

$T_e(\text{O II V1}/[\text{O III}]\lambda 5007)$ was derived using the aforementioned O II V1 intensities with respect to $[\text{O III}]\lambda 5007$ and is presented in the second column of Table A7 for each object of our sample. The O II V1/ $[\text{O III}]\lambda 5007$ line intensity ratio depends on the electron temperature in a different proportion than $[\text{O III}] \lambda 4363/\lambda 5007$, given the different dependence of the emissivities of O II V1 and $[\text{O III}] \lambda 4363$ lines with T_e . If we assume that both RLs and CELs arise from the same ionized gas, the difference between $T_e(\text{O II V1}/[\text{O III}]\lambda 5007)$ and $T_e([\text{O III}] \lambda 4363/\lambda 5007)$ give us an estimate of the temperature inhomogeneities. It should be noted that the derived $T_e(\text{O II V1}/[\text{O III}]\lambda 5007)$ is the temperature value that eliminates the discrepancy between the $n(\text{O}^{2+})/n(\text{H}^+)$ ratio derived with CELs and RLs. Using the formalism of [10] -Eqs. (10) and (11)-, we calculate $T_0(\text{O}^{2+})$ and $t^2(\text{O}^{2+})$. It is important to highlight that the ADF is not synonymous with t^2 . $\text{ADF}(\text{O}^{2+})$ is the consequence of an inhomogeneous temperature structure affecting $T_e([\text{O III}] \lambda 4363/\lambda 5007)$ and therefore both quantities are intrinsically related and described by both $T_0(\text{O}^{2+})$ and $t^2(\text{O}^{2+})$ [2].

In the first part of this article, we show a tight relationship between $t^2(\text{O}^{2+})$ and $\Delta T_e = T_e([\text{O III}] \lambda 4363/\lambda 5007) - T_e([\text{N II}] \lambda 5755/\lambda 6584)$. As mentioned, this is a consequence of the fact that $T_e([\text{N II}] \lambda 5755/\lambda 6584)$ is linearly correlated with $T_0(\text{O}^{2+})$ (or $T_e(\text{O II V1}/[\text{O III}]\lambda 5007)$ as they are practically equivalent in the analyzed H II regions). Therefore, Fig. 1 and Fig. 2 are complementary. Mathematically, the formalism of [10] predicts the linear fit shown in Eq. (3) with the presence of any phenomenon that produces $T_e([\text{O III}] \lambda 4363/\lambda 5007) > T_e(\text{O II V1}/[\text{O III}]\lambda 5007)$ (and consequently $\text{ADF}(\text{O}^{2+}) > 0$) and preserves the linearity between $T_0(\text{O}^{2+})$ and $T_e([\text{N II}] \lambda 5755/\lambda 6584)$. Temperature inhomogeneities in the volume of high degree of ionization is the only paradigm that fulfill these requirements as other explanations to the $\text{ADF}(\text{O}^{2+})$ would imply the invalidity of $T_e(\text{O II V1}/[\text{O III}]\lambda 5007)$ as a real temperature diagnostic. We discard other explanations to the $\text{ADF}(\text{O}^{2+})$ in H II regions from the literature as follows:

- If there were chemical inhomogeneities, they would create temperature variations. Nevertheless, in that case, $T_e(\text{O II V1}/[\text{O III}]\lambda 5007)$ would not correlate with $T_e([\text{N II}] \lambda 5755/\lambda 6584)$ as the volumes emitting RLs and CELs would be different [39].
- If the $\text{ADF}(\text{O}^{2+})$ were created by fluorescent excitation of the O II V1 RLs, then these lines would be enhanced in proportion to parameters different than the electron temperature of the gas (such as the effective temperature of the ionizing star or the optical depth). Therefore $T_e(\text{O II V1}/[\text{O III}]\lambda 5007)$ and $T_e([\text{N II}] \lambda 5755/\lambda 6584)$ would not correlate.
- If the free electrons follow a kappa distribution instead of a Maxwellian one, supra-thermal electrons would create temperature variations that can be directly described by t^2 . However, both observational and theoretical evidence indicate the prevalence of a Maxwellian distribution of velocities [40].
- In the case of errors in the recombination coefficients of the O II V1 RLs, the observed $\text{ADF}(\text{O}^{2+})$ would be approximately constant [4], which is not the case.
- In order to have an important recombination contribution to the auroral [O III] $\lambda 4363$ line intensity, a large fraction of O^{3+}/O is required. This is not the case in the analyzed H II regions. Moreover, Fig. 6 shows that $t^2(\text{O}^{2+})$ and $T_e([\text{Ar III}] \lambda 5192/\lambda 7751) - T_e([\text{N II}] \lambda 5755/\lambda 6584)$ also have a correlation despite of the larger scatter.

To ensure that our conclusions are free of selection bias, we searched for spectra of extragalactic H II regions in the literature that follow the same selection criteria of our study. Due to the difficulty of simultaneously observing [N II] $\lambda 5755$, [O III] $\lambda 4363$ and the O II V1 RLs, there are not many candidates. We study the 9 spectra presented in Table A3 by analyzing them with the same methodology as for the rest of the nebulae. In Fig. 7 we show that our conclusions do not depend on the adopted sample as the H II regions from the literature follow the same trend.

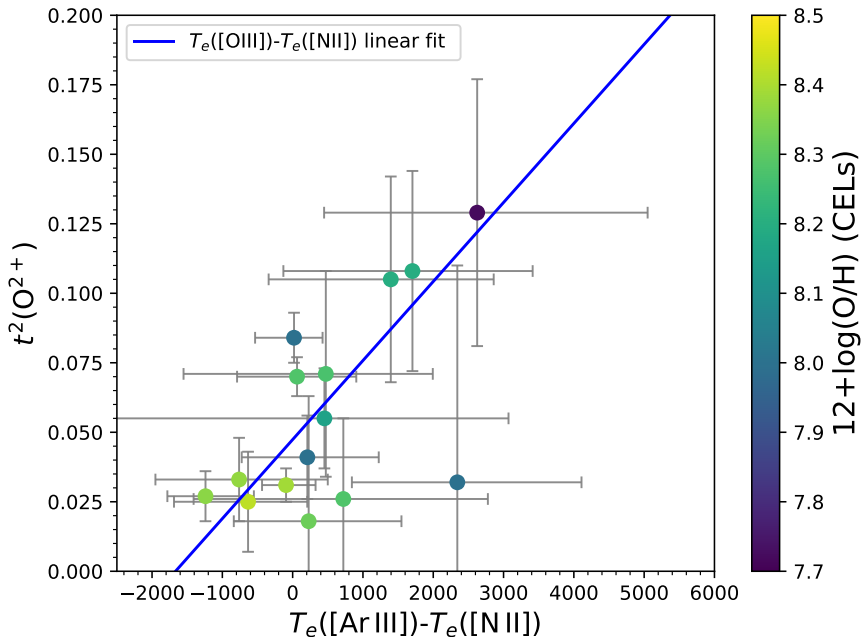


Fig. 6 $t^2(\text{O}^{2+})$ compared with $T_e([\text{Ar III}] \lambda 5192/\lambda 7751) - T_e([\text{N II}] \lambda 5755/\lambda 6584)$ for the studied sample of extragalactic H II regions.

In Table A8 we present the O^+/H^+ (CELs), O^{2+}/H^+ (CELs) and O^{2+}/H^+ (RLs) ratios. The ionic abundances are derived with the *getIonAbundance* task of PyNeb. In the case of O^+/H^+ , we use the $[\text{O II}] \lambda 3726 + 29$ intensity and $T_e([\text{N II}] \lambda 5755/\lambda 6584)$. To derive O^{2+}/H^+ (CELs), we use $[\text{O III}] \lambda 5007$ and $T_e([\text{O III}] \lambda 4363/\lambda 5007)$, whereas to derive O^{2+}/H^+ (RLs) we use the O II V1 intensity and $T_e([\text{O III}] \lambda 4363/\lambda 5007)$ (the temperature dependence is negligible). As HI RLs are emitted both in the high and low ionization volumes, we can apply the following relation [41]:

$$T_0(\text{H}^+) \approx \frac{T_0(\text{O}^+) \times n(\text{O}^+) + T_0(\text{O}^{2+}) \times n(\text{O}^{2+})}{n(\text{O}^+) + n(\text{O}^{2+})}, \quad (6)$$

where $T_0(\text{O}^+)$ and $n(\text{O}^+)$ are the average temperature and particle density of O^+ , respectively. As our results show that $T_e([\text{N II}] \lambda 5755/\lambda 6584) \approx T_0(\text{O}^+)$, we can infer a $T_0(\text{H}^+)$ -metallicity relation, as is presented in Fig. 8 and Eq. (7). This last relation is very important as it permits to estimate the metallicity from radio observations, where it is possible to measure $T_e(\text{HI})$.

$$12 + \log(\text{O}/\text{H}) = (-1.07 \pm 0.09) \times 10^{-4} T_0(\text{H}^+) + (9.44 \pm 0.08) \text{ (K)}. \quad (7)$$

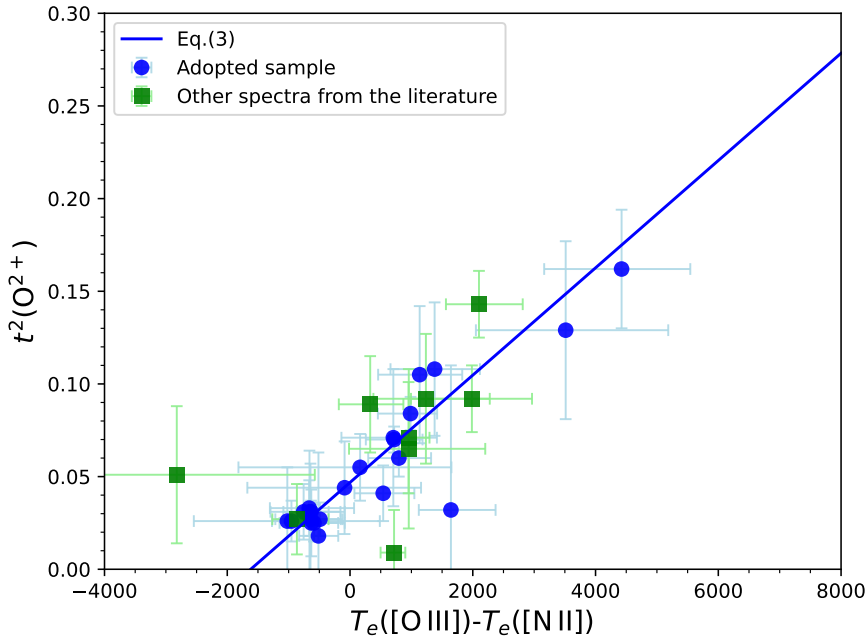


Fig. 7 $t^2(\text{O}^{2+})$ versus ΔT_e for the extragalactic H II regions of our sample (blue dots) and those from the literature presented in Table A3 (green squares).

When $T_e([\text{N II } \lambda 5755/\lambda 6584]) \approx T_0(\text{O}^+)$ is considered, Eq. (6) shows that it is possible to get $T_0(\text{H}^+)$ values which are close to $T_e([\text{O III } \lambda 4363/\lambda 5007])$ even if $t^2(\text{O}^{2+}) > 0$. This is due to the fact that in the regions of low degree of ionization, the emission of H I R_Ls will come essentially from the volume of O^+ , where temperature inhomogeneities are negligible. On the other hand, $T_e([\text{N II } \lambda 5755/\lambda 6584]) \approx T_0(\text{O}^+)$ have larger values than $T_0(\text{O}^{2+})$ (see Fig. (2)). Therefore, finding some nebulae where $T_e(\text{H I}) \approx T_e([\text{O III } \lambda 4363/\lambda 5007])$ is not an argument against the existence of temperature inhomogeneities. In Fig. 9 we show that in some regions of our sample we could expect that $T_e(\text{H I}) \approx T_e([\text{O III } \lambda 4363/\lambda 5007])$ even if $t^2(\text{O}^{2+}) > 0$.

An important point to mention is the possible existence of $\text{ADF}(\text{O}^+)$. To date, there are no reported $\text{ADF}(\text{O}^+)$ (or from any ion of low degree of ionization) in extragalactic H II regions. The available cases are limited to Galactic planetary nebulae (PNe) and 3 Galactic H II regions: M8, M20 and the Orion Nebula [12]. Besides the possible contribution of sky contamination in the O I 7773+ multiplet, it is necessary to study the aperture effects on these nebulae, since echelle observations [42–44] are limited to very small areas of the nebula. For instance, in the dense gas of the Orion Nebula, a high density clump (such as a proplyd or an Herbig-Haro object) can create a fake local peak of $T_e([\text{N II } \lambda 5755/\lambda 6584])$ [45, 46], giving the n_e -sensitivity of $[\text{N II } \lambda 5755/\lambda 6584]$

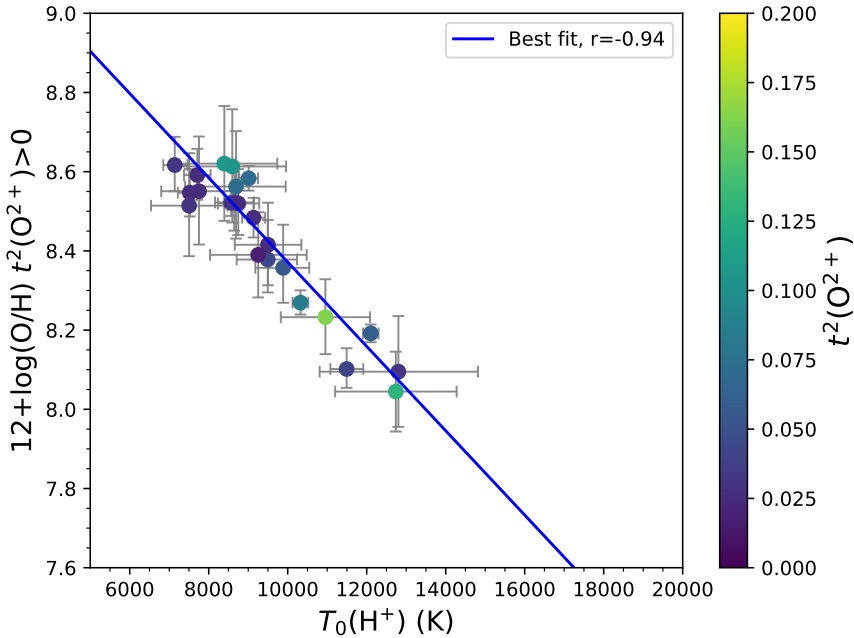


Fig. 8 $T_0(\text{H}^+)$ -metallicity relation considering $t^2(\text{O}^{2+}) > 0$ for our sample of extragalactic H II regions.

at values higher than 1000 cm^{-3} . In any case, the $\text{ADF}(\text{O}^+)$ could have a negligible effect on the integrated spectrum where the entire temperature structure is encompassed. If a large $\text{ADF}(\text{O}^+)$ exists in extragalactic H II regions, this work shows that the main cause would not be temperature inhomogeneities. But before discussing a problem, we need evidence that it really exists.

Finally, we explore the effect of temperature inhomogeneities on the PNe shown in Table A5 following the same methodology described for H II regions. Fig. 10 shows that, in general, PNe do not follow the same trend between $t^2(\text{O}^{2+})$ and ΔT_e as H II regions. It should be noted that the ionizing sources of these objects are hotter, having a considerable fraction of O^{3+}/O . Therefore the heating may be affecting mainly the O^{3+} volume, which is not accessible in the optical range. Furthermore, there are strong indications that some PNe with binary central stars can have inclusions of (at least) two distinct gas components with different metallicities [47–51]. These chemical inhomogeneities also produce temperature variations, but they imply the invalidity of $t^2(\text{O}^{2+})$ derived from $T_e(\text{O II V1}/[\text{O III}]\lambda 5007)$ as the emission of RLs and CELs would come from non related volumes [39]. This is particularly important in the extreme ADF PNe Ou5 and Abell 46 [52]. The abundance discrepancy problem in PNe remains open and requires further investigations, although [53] found that the effect of temperature inhomogeneities on these objects is not negligible.

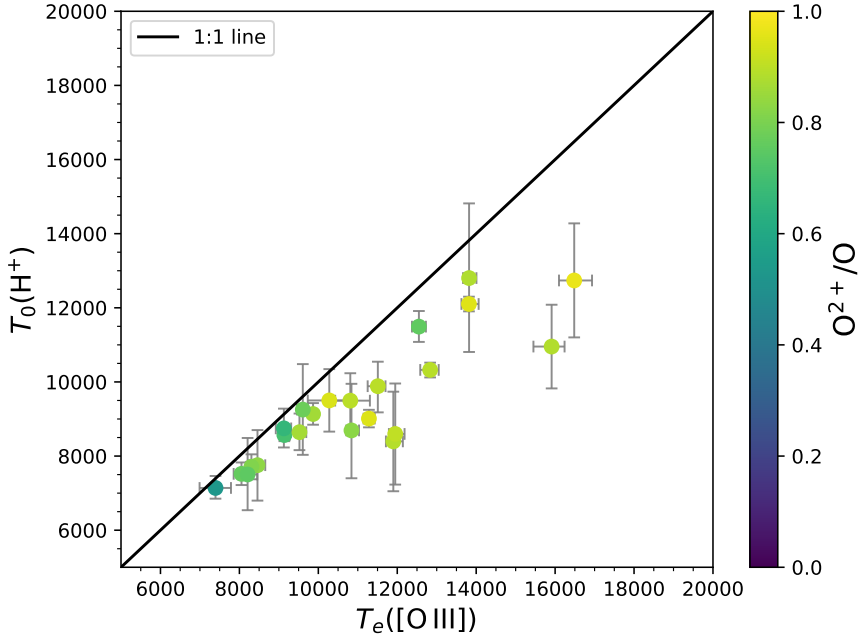


Fig. 9 Comparison between $T_e([\text{O III}] \lambda 4363/\lambda 5007)$ and $T_0(\text{H}^+)$, which was derived using Eq. (6) for our sample of extragalactic H II regions.

Table 1 Adopted atomic data set.

Ion	Transition Probabilities	Collision Strengths	Effective recombination coefficients
H ⁺	-	-	[54]
O ⁺	[30]	[31]	-
O ²⁺	[55], [56]	[57]	[11]
N ⁺	[30]	[58]	-
S ⁺	[28]	[29]	-
Cl ²⁺	[32]	[33]	-
Ar ²⁺	[59], [60]	[61]	-
Ar ³⁺	[34]	[35]	-
Fe ²⁺	[36]	[37]	-

Acknowledgments. JEM-D appreciates the fruitful conversations with Antonio Peimbert and Silvia Torres-Peimbert on the formalism of temperature variations and chemical inhomogeneities in the ionized gas. JEM-D acknowledges interesting discussions with William J. Henney.

Authors' contributions. JEM-D conducted the study with the original idea, compiled the appropriate data, re-calculated the physical conditions and chemical abundances, wrote the text, created the figures and interpreted the results. CE, JG-R, KK and MP reviewed the consistency of the analysis, the

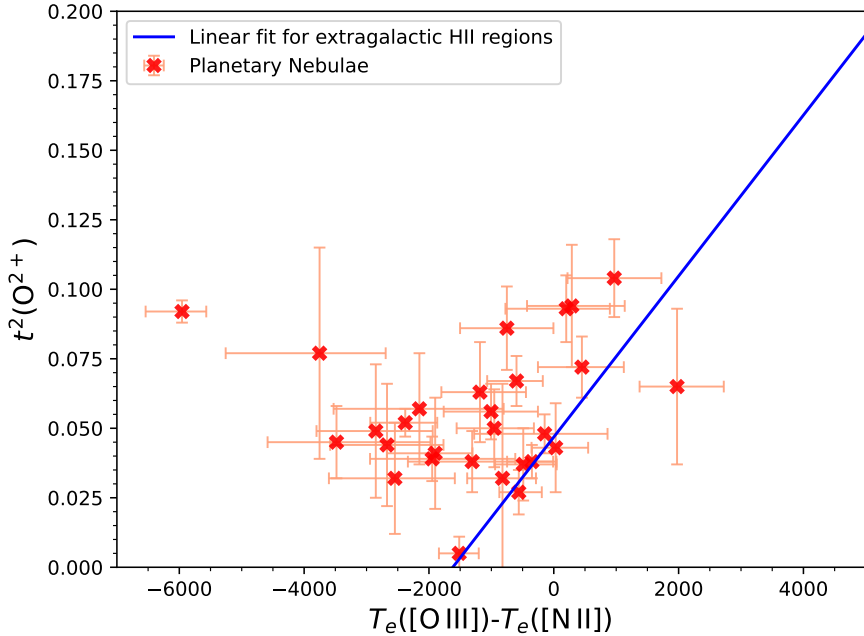


Fig. 10 $t^2(\text{O}^{2+})$ versus ΔT_e relation for Galactic planetary nebulae.

formalism of temperature fluctuations, contributed to data interpretation and discussion, and modified the text. The participation of all the authors was essential for the realization of this work.

Conflict of interest/Competing interests. The authors declare that they have no competing financial interests.

Data availability. All the data is public and available in cited the references. Our calculations are entirely present in Tables A1-A8.

Funding. JEM-D and KK gratefully acknowledge funding from the Deutsche Forschungsgemeinschaft (DFG, German Research Foundation) in the form of an Emmy Noether Research Group (grant number KR4598/2-1, PI Kreckel). CE and JG-R acknowledge support from the Agencia Estatal de Investigación del Ministerio de Ciencia e Innovación (AEI-MCINN) under grant *Espectroscopía de campo integral de regiones H II locales. Modelos para el estudio de regiones H II extragalácticas* with reference 10.13039/501100011033 and support under grant P/308614 financed by funds transferred from the Spanish Ministry of Science, Innovation and Universities, charged to the General State Budgets and with funds transferred from the General Budgets of the Autonomous Community of the Canary Islands by the MCIU. JG-R acknowledges support from an Advanced Fellowship under the Severo Ochoa excellence program CEX2019-000920-S and financial support from the Canarian Agency for Research, Innovation and Information Society (ACIISI), of the Canary

Islands Government, and the European Regional Development Fund (ERDF), under grant with reference ProID2021010074.

Additional Information. Correspondence should be addressed to JEM-D: jemd@uni-heidelberg.de

Appendix A Physical conditions, ionic abundances and references

References

- [1] Wyse, A.B.: The Spectra of Ten Gaseous Nebulae. *ApJ* **95**, 356 (1942). <https://doi.org/10.1086/144409>
- [2] Peimbert, M.: Temperature Determinations of H II Regions. *ApJ* **150**, 825 (1967). <https://doi.org/10.1086/149385>
- [3] Torres-Peimbert, S., Peimbert, M., Pena, M.: Planetary nebulae with a high degree of ionization : NGC 2242 and NGC 4361. *A&A* **233**, 540 (1990)
- [4] Rodríguez, M., García-Rojas, J.: Temperature Structure and Metallicity in H II Regions. *ApJ* **708**(2), 1551–1559 (2010) [arXiv:0912.0302](https://arxiv.org/abs/0912.0302) [astro-ph.GA]. <https://doi.org/10.1088/0004-637X/708/2/1551>
- [5] Nicholls, D.C., Dopita, M.A., Sutherland, R.S.: Resolving the Electron Temperature Discrepancies in H II Regions and Planetary Nebulae: κ -distributed Electrons. *ApJ* **752**(2), 148 (2012) [arXiv:1204.3880](https://arxiv.org/abs/1204.3880) [astro-ph.GA]. <https://doi.org/10.1088/0004-637X/752/2/148>
- [6] Rubin, R.H.: Noncollisional Excitation of Low-lying States in Gaseous Nebulae. *ApJ* **309**, 334 (1986). <https://doi.org/10.1086/164606>
- [7] Peimbert, M., Peimbert, A., Delgado-Inglada, G.: Nebular Spectroscopy: A Guide on Hii Regions and Planetary Nebulae. *PASP* **129**(978), 082001 (2017) [arXiv:1705.06323](https://arxiv.org/abs/1705.06323) [astro-ph.GA]. <https://doi.org/10.1088/1538-3873/aa72c3>
- [8] García-Rojas, J.: Physical Conditions and Chemical Abundances in Photoionized Nebulae from Optical Spectra. In: *Reviews in Frontiers of Modern Astrophysics; From Space Debris to Cosmology*, pp. 89–121 (2020). https://doi.org/10.1007/978-3-030-38509-5_4
- [9] Peimbert, M., Costero, R.: Chemical Abundances in Galactic HII Regions. *Boletín de los Observatorios Tonantzintla y Tacubaya* **5**, 3–22 (1969)

Table A1 Physical conditions for our sample of extragalactic H II regions.

Region	$n_e([\text{O II}])$ cm^{-3}	$n_e([\text{S II}])$ cm^{-3}	Adop. n_e cm^{-3}	$T_e([\text{O III}])$ K	$T_e([\text{Ar III}])$ K	$T_e([\text{N II}])$ K	Ref.
NGC 5461	310^{+90}_{-80}	220^{+110}_{-120}	270 ± 100	8460^{+200}_{-220}	-	9100^{+300}_{-350}	[62]
NGC 588	90^{+110}_{-70}	150^{+120}_{-110}	120^{+110}_{-90}	10810^{+500}_{-380}	-	10900^{+1750}_{-1200}	[63]
NGC 595	60 ± 20	40 ± 30	< 100	7390^{+380}_{-400}	-	8150^{+210}_{-140}	[62]
K 932	250 ± 30	110 ± 50	180 ± 40	8300^{+140}_{-130}	-	9260^{+170}_{-190}	[62]
IC 132	160^{+200}_{-110}	200^{+170}_{-120}	180^{+180}_{-120}	10280^{+450}_{-540}	12020^{+1000}_{-1150}	11300^{+1050}_{-980}	[63]
N 11B	290 ± 100	260^{+60}_{-50}	270 ± 80	9140^{+130}_{-90}	9680^{+260}_{-190}	9780^{+160}_{-150}	[38]
NGC 5471	210^{+60}_{-50}	170^{+70}_{-60}	190^{+60}_{-50}	13820^{+190}_{-150}	14520^{+1220}_{-1130}	12180^{+540}_{-370}	[64]
N 66A	180^{+100}_{-90}	180 ± 70	180 ± 80	12550 ± 180	12220^{+690}_{-640}	12010^{+330}_{-290}	[38]
NGC 604	60 ± 20	50^{+40}_{-30}	< 100	8050^{+140}_{-200}	-	8640^{+260}_{-240}	[62]
NGC 6822	150^{+100}_{-90}	110^{+90}_{-70}	130^{+100}_{-80}	11510^{+190}_{-260}	11800^{+1330}_{-1420}	11340^{+1290}_{-1720}	[65]
UV-1	190 ± 70	280 ± 80	240 ± 80	10840^{+190}_{-130}	10610^{+1000}_{-1310}	10130^{+520}_{-710}	[66]
NGC 5408	220 ± 90	200^{+110}_{-90}	210^{+100}_{-90}	15910^{+330}_{-460}	-	11490^{+790}_{-800}	[65]
NGC 1714	450^{+140}_{-130}	340^{+140}_{-130}	390^{+140}_{-130}	9520^{+170}_{-220}	9430^{+700}_{-770}	10190^{+560}_{-430}	[38]
N 81	440 ± 130	340^{+80}_{-90}	390^{+100}_{-110}	12830^{+250}_{-250}	11870^{+190}_{-270}	11850^{+320}_{-280}	[38]
IC 2111	290 ± 120	240^{+120}_{-100}	270^{+120}_{-110}	9130^{+180}_{-200}	9120^{+480}_{-450}	9760^{+360}_{-310}	[38]
NGC 2363	270^{+90}_{-100}	170^{+120}_{-90}	220^{+110}_{-100}	16480^{+450}_{-390}	15600^{+1200}_{-1100}	12970^{+1220}_{-1080}	[62]
30Dor	440 ± 20	350 ± 20	390 ± 20	9870^{+90}_{-40}	9120^{+400}_{-300}	10360^{+280}_{-240}	[67]
N 44C	190^{+110}_{-80}	100 ± 50	140^{+80}_{-70}	11280^{+150}_{-140}	10630 ± 530	10560^{+320}_{-330}	[38]
HII-2	420^{+110}_{-90}	380^{+100}_{-90}	400^{+110}_{-90}	11900^{+240}_{-190}	12230^{+1210}_{-1300}	10520^{+500}_{-530}	[66]
NGC 5455	240^{+60}_{-50}	160 ± 50	200 ± 50	9610^{+120}_{-150}	10350^{+1120}_{-900}	10120^{+200}_{-170}	[64]
VS44	150 ± 20	100^{+30}_{-40}	< 100	8210^{+240}_{-170}	-	8870^{+330}_{-250}	[62]
N 88A	2700^{+570}_{-400}	1840^{+400}_{-310}	3130 ± 1120	13820^{+250}_{-190}	20190^{+680}_{-670}	13020^{+280}_{-310}	[38]
HII-1	360 ± 90	420^{+110}_{-90}	390^{+100}_{-90}	11950^{+240}_{-160}	12210^{+1010}_{-1220}	10810^{+460}_{-520}	[66]

Table A2 Physical conditions of the adopted sample of Galactic ring nebulae.

Region	n_e ([S II]) cm ⁻³	T_e ([O III]) K	T_e ([Ar III]) K	T_e ([N II]) K	Ref.
NGC 7635A2	120 ± 40	8130 ⁺⁴⁰⁰ ₋₅₅₀	-	8000 ⁺⁵⁶⁰ ₋₆₀₀	[19]
NGC 7635A3	90 ⁺⁵⁰ ₋₄₀	7530 ⁺⁶¹⁰ ₋₅₂₀	-	8190 ⁺⁴²⁰ ₋₃₀₀	[19]
NGC 7635A4	1450 ⁺¹³⁰ ₋₁₄₀	8650 ⁺³⁵⁰ ₋₄₈₀	8410 ⁺⁷²⁰ ₋₈₁₀	9010 ⁺¹¹⁰ ₋₉₀	[19]
NGC 6888A2	290 ± 80	12710 ⁺⁴⁰⁰ ₋₄₁₀	-	7380 ± 110	[19]
NGC 6888A3	210 ⁺¹⁰⁰ ₋₈₀	10040 ⁺⁵⁰⁰ ₋₈₇₀	-	7570 ⁺¹⁶⁰ ₋₁₈₀	[19]
NGC 6888A4	120 ⁺⁸⁰ ₋₆₀	10050 ⁺⁸²⁰ ₋₉₃₀	-	8800 ⁺²⁰⁰ ₋₁₁₀	[19]
NGC 6888A5	170 ± 70	9850 ⁺⁴²⁰ ₋₅₈₀	7310 ⁺⁷⁴⁰ ₋₆₁₀	8660 ⁺²²⁰ ₋₂₄₀	[19]
NGC 6888A6	180 ⁺¹⁰⁰ ₋₉₀	9620 ⁺⁶²⁰ ₋₈₇₀	-	8660 ⁺²¹⁰ ₋₁₆₀	[19]

- [10] Peimbert, A., Peimbert, M.: Densities, Temperatures, Pressures, and Abundances Derived from O II Recombination Lines in H II Regions and their Implications. *ApJ* **778**(2), 89 (2013) [arXiv:1310.0089](https://arxiv.org/abs/1310.0089) [astro-ph.GA]. <https://doi.org/10.1088/0004-637X/778/2/89>
- [11] Storey, P.J., Sochi, T., Bastin, R.: Recombination coefficients for O II lines in nebular conditions. *MNRAS* **470**(1), 379–389 (2017) [arXiv:1703.09982](https://arxiv.org/abs/1703.09982) [physics.atom-ph]. <https://doi.org/10.1093/mnras/stx1189>
- [12] García-Rojas, J., Esteban, C.: On the Abundance Discrepancy Problem in H II Regions. *ApJ* **670**(1), 457–470 (2007) [arXiv:0707.3518](https://arxiv.org/abs/0707.3518) [astro-ph]. <https://doi.org/10.1086/521871>
- [13] Méndez-Delgado, J.E., Amayo, A., Arellano-Córdova, K.Z., Esteban, C., García-Rojas, J., Carigi, L., Delgado-Inglada, G.: Gradients of chemical abundances in the Milky Way from H II regions: distances derived from Gaia EDR3 parallaxes and temperature inhomogeneities. *MNRAS* **510**(3), 4436–4455 (2022) [arXiv:2112.12600](https://arxiv.org/abs/2112.12600) [astro-ph.GA]. <https://doi.org/10.1093/mnras/stab3782>
- [14] Esteban, C., Peimbert, M., Torres-Peimbert, S., Rodríguez, M.: Optical Recombination Lines of Heavy Elements in Giant Extragalactic H II Regions. *ApJ* **581**(1), 241–257 (2002) [arXiv:astro-ph/0208313](https://arxiv.org/abs/astro-ph/0208313) [astro-ph]. <https://doi.org/10.1086/344104>
- [15] Peimbert, A., Peña-Guerrero, M.A., Peimbert, M.: A Classification of H II Regions Based on Oxygen and Helium Lines: The Cases of TOL 2146-391 and TOL 0357-3915. *ApJ* **753**(1), 39 (2012) [arXiv:1204.4507](https://arxiv.org/abs/1204.4507) [astro-ph.CO]. <https://doi.org/10.1088/0004-637X/753/1/39>
- [16] Toribio San Cipriano, L., Domínguez-Guzmán, G., Esteban, C., García-Rojas, J., Mesa-Delgado, A., Bresolin, F., Rodríguez, M., Simón-Díaz, S.: Carbon and oxygen in H II regions of the Magellanic Clouds: abundance

Table A3 Physical conditions of the extragalactic H II regions from other research groups.

Region	$n_e([\text{O II}])$ cm^{-3}	$n_e([\text{S II}])$ cm^{-3}	Adop. n_e cm^{-3}	$T_e([\text{O III}])$ K	$T_e([\text{Ar III}])$ K	$T_e([\text{N II}])$ K	Ref.
NGC 456a-1	-	290^{+40}_{-50}	290^{+40}_{-50}	12210^{+70}_{-130}	-	11890^{+470}_{-380}	[68]
NGC 456a-2	-	80^{+40}_{-30}	< 100	11940^{+70}_{-100}	-	10700^{+980}_{-760}	[68]
NGC 6822V	70^{+50}_{-30}	90^{+70}_{-50}	< 100	11700^{+280}_{-210}	-	14520^{+1970}_{-2280}	[69]
NGC 5253C1	-	530^{+70}_{-50}	530^{+70}_{-50}	12140^{+80}_{-70}	-	11420^{+100}_{-150}	[68]
Mrk1259	-	780^{+80}_{-70}	780^{+80}_{-70}	9970^{+460}_{-280}	-	7860^{+250}_{-280}	[68]
NGC 5253C2	-	200 ± 40	200 ± 40	10150^{+50}_{-80}	-	11010^{+440}_{-350}	[68]
NGC 5253P2	-	810 ± 80	810 ± 80	12280^{+120}_{-140}	-	11320^{+320}_{-240}	[68]
NGC 346	40^{+30}_{-20}	40^{+30}_{-20}	< 100	12820^{+120}_{-170}	-	10830^{+860}_{-880}	[70]
NGC 456-2	210 ± 20	210 ± 50	210 ± 40	12070^{+170}_{-220}	11320^{+1250}_{-1150}	11110^{+1070}_{-760}	[71]

Table A4 Electron density values of the adopted sample of Galactic H II regions.

Region	$n_e(\text{[O II]})$ cm ⁻³	$n_e(\text{[S II]})$ cm ⁻³	$n_e(\text{[Fe III]})$ cm ⁻³	$n_e(\text{[Cl III]})$ cm ⁻³	$n_e(\text{[Ar IV]})$ cm ⁻³	Adop. n_e cm ⁻³	Ref.
NGC 3603	2600 ⁺⁸⁰⁰ ₋₅₁₀	2890 ⁺¹¹⁴⁰ ₋₆₅₀	8400 ⁺²⁸³⁶⁰ ₋₅₅₀₀	4850 ⁺¹³⁵⁰ ₋₁₅₇₀	1950 ⁺¹⁶²⁰ ₋₁₂₁₀	2850 ± 750	[43]
M42-P1	4700 ⁺⁹⁵⁰ ₋₈₇₀	2870 ⁺⁶⁷⁰ ₋₆₀₀	6590 ⁺³²⁰⁰ ₋₂₀₁₀	5930 ⁺¹³⁸⁰ ₋₁₀₂₀	5920 ⁺³⁸⁰⁰ ₋₃₃₁₀	3990 ± 1280	[72]
M42-2	5850 ⁺⁸²⁰ ₋₇₇₀	3760 ⁺¹³⁹⁰ ₋₇₅₀	10340 ⁺²¹⁸⁰ ₋₂₁₃₀	7510 ⁺⁸²⁰ ₋₆₄₀	6690 ⁺⁵⁸⁰ ₋₄₈₀	6500 ± 1240	[73]
Sh 2-100	-	390 ⁺²³⁰ ₋₁₇₀	13340 ⁺²¹⁹⁷⁰ ₋₉₇₂₀	750 ⁺⁴¹⁰ ₋₃₃₀	-	390 ⁺²³⁰ ₋₁₇₀	[74]
M42-3	5320 ⁺⁷¹⁰ ₋₅₅₀	4100 ⁺¹¹⁶⁰ ₋₉₅₀	11300 ⁺³⁴¹⁰ ₋₂₃₃₀	7310 ⁺⁹⁰⁰ ₋₈₃₀	5950 ⁺¹⁴¹⁰ ₋₁₁₇₀	5810 ± 1350	[75]
M42-1	5340 ⁺⁷²⁰ ₋₅₆₀	4180 ⁺¹⁰²⁰ ₋₈₀₀	10310 ⁺²⁸⁵⁰ ₋₂₆₇₀	6900 ⁺⁷²⁰ ₋₆₁₀	4190 ⁺¹³⁸⁰ ₋₁₂₇₀	5670 ± 1260	[75]
Sh 2-311	270 ⁺⁸⁰ ₋₆₀	300 ± 100	6420 ⁺¹⁷¹⁶⁰ ₋₄₈₉₀	-	-	290 ⁺⁹⁰ ₋₈₀	[76]
M16	1160 ⁺²¹⁰ ₋₁₉₀	1080 ⁺²²⁰ ₋₁₉₀	10160 ⁺²⁰³⁰⁰ ₋₈₁₈₀	1190 ⁺⁵³⁰ ₋₅₁₀	-	1130 ± 100	[43]
M42-bar	4200 ⁺⁴⁹⁰ ₋₄₁₀	3240 ⁺⁷⁵⁰ ₋₅₇₀	4240 ⁺²⁰¹⁰ ₋₁₇₉₀	4330 ⁺⁵⁵⁰ ₋₆₄₀	30870 ⁺⁴⁸⁴⁰⁰ ₋₂₃₆₁₀	4030 ± 480	[72]
M42-1	1110 ⁺⁸⁰ ₋₉₀	1320 ⁺¹⁷⁰ ₋₁₉₀	4120 ⁺¹²⁶⁰ ₋₁₃₅₀	1540 ⁺²⁴⁰ ₋₂₄₀	-	1190 ± 190	[46]
NGC 3576	1710 ⁺²⁶⁰ ₋₂₈₀	1050 ⁺³⁰⁰ ₋₂₇₀	1560 ⁺¹³⁵⁰ ₋₁₃₈₀	2890 ⁺⁶³⁰ ₋₆₂₀	3050 ⁺¹⁶²⁰ ₋₁₃₈₀	1560 ± 550	[77]
M42	6790 ⁺²⁵¹⁰ ₋₁₆₂₀	4550 ⁺³¹⁵⁰ ₋₁₅₀₀	9550 ⁺³⁵⁷⁰ ₋₂₈₂₀	7020 ⁺⁶¹⁰ ₋₅₄₀	4810 ⁺¹¹⁹⁰ ₋₉₀₀	6510 ± 1060	[42]
M17	500 ⁺¹¹⁰ ₋₁₀₀	380 ± 110	9560 ⁺³²⁸⁰⁰ ₋₇₃₃₀	370 ⁺²⁷⁰ ₋₂₀₀	-	440 ⁺¹¹⁰ ₋₁₀₀	[44]
M8	1630 ⁺⁶⁷⁰ ₋₅₀₀	1230 ⁺²¹⁰ ₋₁₇₀	2440 ⁺¹⁸¹⁰ ₋₁₁₃₀	1870 ⁺²³⁰ ₋₂₇₀	4140 ⁺³²³⁰ ₋₂₈₀₀	1480 ± 330	[44]
M42-4	4860 ⁺⁶²⁰ ₋₅₁₀	3980 ⁺⁷⁹⁰ ₋₆₆₀	9660 ⁺³⁰⁹⁰ ₋₂₂₃₀	6970 ⁺⁶⁷⁰ ₋₆₃₀	5220 ⁺⁸²⁰ ₋₇₁₀	5360 ± 1200	[75]
M42-3	5350 ⁺⁷²⁰ ₋₆₃₀	3950 ⁺⁸⁶⁰ ₋₅₇₀	7580 ⁺²⁵⁹⁰ ₋₁₉₅₀	7650 ⁺⁸¹⁰ ₋₇₉₀	4670 ⁺⁵⁰⁰ ₋₄₁₀	5170 ± 1180	[73]
Sh 2-288	-	430 ⁺²⁵⁰ ₋₂₃₀	2960 ⁺⁶⁰⁸⁰ ₋₂₂₄₀	440 ⁺³⁶⁰ ₋₂₇₀	-	430 ⁺²⁵⁰ ₋₂₃₀	[74]
M42	2710 ⁺⁶⁹⁰ ₋₅₄₀	1800 ⁺⁵⁷⁰ ₋₅₂₀	4370 ⁺⁶¹²⁰ ₋₃₀₂₀	2120 ⁺⁹⁷⁰ ₋₈₀₀	89060 ⁺³¹⁷⁷⁴⁰ ₋₆₃₁₁₀	2200 ± 480	[78]
M42-2	1460 ⁺¹⁴⁰ ₋₁₁₀	1160 ⁺¹⁹⁰ ₋₁₄₀	3530 ⁺²³⁴⁰ ₋₁₄₉₀	2000 ⁺⁵⁰⁰ ₋₄₇₀	-	1380 ± 220	[46]
M42-2	5110 ⁺⁶⁶⁰ ₋₅₆₀	4090 ⁺⁸⁹⁰ ₋₇₇₀	10160 ⁺²⁴⁹⁰ ₋₁₉₉₀	6510 ⁺⁶¹⁰ ₋₆₁₀	5870 ± 720	5620 ± 1080	[75]

Table A5 Electron density values of the adopted sample of Galactic planetary nebulae.

Region	$n_e(\text{O II})$ cm ⁻³	$n_e(\text{S II})$ cm ⁻³	$n_e(\text{Fe III})$ cm ⁻³	$n_e(\text{C III})$ cm ⁻³	$n_e(\text{Ar IV})$ cm ⁻³	Adop. n_e cm ⁻³	Ref.
NGC 2440	4080 ⁺⁶²⁰ ₋₅₉₀	2620 ⁺⁴²⁰ ₋₃₈₀	-	5520 ⁺⁵⁵⁰ ₋₅₁₀	5000 ⁺⁶¹⁰ ₋₆₀₀	3990 ± 1220	[79]
Hb 4	7200 ⁺¹³⁴⁷⁰ ₋₂₂₁₀	5200 ⁺⁵⁰¹⁰ ₋₂₇₈₀	-	6930 ⁺¹⁶⁸⁰ ₋₁₁₇₀	7320 ⁺¹¹⁹⁰ ₋₁₃₈₀	7060 ± 520	[80]
NGC 5315	12510 ⁺³²⁰⁰ ₋₆₃₄₀	7920 ⁺¹¹⁵⁹⁰ ₋₄₃₈₀	10730 ⁺¹⁹⁶⁹⁰ ₋₇₂₃₀	34670 ⁺¹¹⁴²⁰ ₋₁₁₄₂₀	37220 ⁺¹⁰²⁷⁰ ₋₈₉₅₀	20930 ± 13320	[81]
M 1-31	15130 ⁺⁹²²⁰ ₋₂₅₆₀	9990 ⁺⁷⁶³⁰ ₋₄₁₈₀	-	19820 ⁺¹⁴²⁹⁰ ₋₉₆₂₀	-	12140 ± 3840	[82]
Cn 1-5	5070 ⁺¹⁴⁹⁰ ₋₁₈₆₇₀	3930 ⁺¹²⁹⁰ ₋₈₃₉₀	14260 ⁺²¹⁸³⁰ ₋₆₃₉₀	3910 ⁺¹⁰¹⁰ ₋₇₀₁₀	10950 ⁺⁶⁹¹⁰ ₋₆₀₂₀	4190 ± 1010	[80]
H 1-40	7790 ⁺⁴¹⁰⁰ ₋₃₇₃₀	8300 ⁺⁴³⁶⁰ ₋₃₄₆₀	16750 ⁺³⁶⁴⁹⁰ ₋₁₂₉₈₀	7630 ⁺⁷⁴²⁰ ₋₅₁₀₀	-	8180 ± 1450	[82]
H 1-50	10670 ⁺⁸⁸⁸⁰ ₋₇₇₀	7160 ⁺⁴³⁰⁰ ₋₂₆₅₀	-	12850 ⁺⁴¹⁷⁰ ₋₃₇₁₀	-	9790 ± 2630	[82]
Hen 2-158	3780 ⁺¹¹⁸⁰ ₋₄₅₂₀	2750 ⁺⁶⁷⁰ ₋₉₈₅₀	12130 ⁺³⁰²³⁰ ₋₉₉₉₀	6470 ⁺⁴¹⁰⁰ ₋₃₆₂₀	18870 ⁺²²³²⁰ ₋₁₂₉₇₀	3220 ± 890	[82]
IC 418	15380 ⁺⁸³⁷⁰ ₋₄₅₂₀	14210 ⁺⁹⁸⁵⁰ ₋₅₆₁₀	-	12200 ⁺¹¹⁵⁰ ₋₁₂₁₀	5130 ⁺⁴⁰²⁰ ₋₂₉₉₀	11640 ± 2220	[83]
PC 14	4520 ⁺¹⁶³⁰ ₋₁₃₀₀	3070 ⁺¹⁶⁴⁰ ₋₉₆₀	-	3410 ⁺⁸⁶⁰ ₋₈₃₀	4710 ⁺¹¹²⁰ ₋₁₁₄₀	3820 ± 660	[80]
M 1-32	9570 ⁺¹⁴³⁶⁰ ₋₅₂₂₀	5940 ⁺¹²⁴²⁰ ₋₃₁₉₀	20710 ⁺²⁰²⁹⁰ ₋₁₀₃₀₀	13460 ⁺³⁶²⁰ ₋₃₁₁₀	-	12350 ± 3120	[80]
M 1-61	19180 ⁺²⁵⁶⁵⁰ ₋₉₇₀₀	9820 ⁺¹⁴²¹⁰ ₋₅₁₀₀	20290 ⁺³⁴¹³⁰ ₋₁₆₃₄₀	19550 ⁺⁵⁴²⁰ ₋₃₅₁₀	33540 ⁺⁹⁶⁰⁰ ₋₆₅₇₀	20900 ± 6910	[80]
Ou 5	1380 ⁺⁵¹⁰ ₋₃₉₀	220 ⁺²²⁰ ₋₁₅₀	-	-	1200 ⁺³⁶⁰ ₋₈₂₀	800 ⁺²⁷⁰ ₋₂₇₀	[52]
NGC 6369	3940 ⁺¹⁵⁴⁰ ₋₁₀₆₀	3170 ⁺¹⁵³⁰ ₋₁₀₀₀	-	4160 ⁺⁹⁷⁰ ₋₁₀₁₀	4960 ⁺¹⁴¹⁰ ₋₁₁₆₀	4070 ± 600	[80]
Pe 1-1	21170 ⁺³³²⁴⁰ ₋₁₁₇₅₀	9850 ⁺⁹⁸³⁰ ₋₄₆₇₀	-	31030 ⁺¹²²⁹⁰ ₋₈₄₈₀	-	17080 ± 9670	[80]
IC 2501	16950 ⁺⁸⁷⁷⁰ ₋₅₁₇₀	8340 ⁺³⁵¹⁰ ₋₁₉₁₀	-	9970 ⁺⁹⁹⁰ ₋₉₆₀	8490 ⁺⁷⁷⁰ ₋₆₆₀	9030 ± 970	[79]
M 1-30	4480 ⁺³⁰²⁰ ₋₁₅₅₀	5160 ⁺⁶¹³⁰ ₋₂₄₂₀	9530 ⁺¹⁷²³⁰ ₋₇₇₈₀	7380 ⁺¹²⁴⁰ ₋₁₄₅₀	-	6560 ± 1300	[80]
IC 4191	14150 ⁺³²⁷⁰ ₋₂₃₃₄₀	7620 ⁺²⁸³⁰ ₋₁₉₃₀	-	14290 ⁺¹⁵⁵⁰ ₋₀₉₈₀	11310 ⁺¹⁰⁹⁰ ₋₀₈₈₀	11990 ± 2020	[79]
Hen 2-96	13340 ⁺²⁵³⁴⁰ ₋₆₃₁₀	8980 ⁺⁶¹³⁰ ₋₃₂₉₀	-	23960 ⁺²⁷⁹⁸⁰ ₋₁₃₇₇₀	38610 ⁺²⁸⁹⁸⁰ ₋₁₈₁₇₀	10980 ± 6050	[82]
M 3-15	9780 ⁺²⁷⁴⁹⁰ ₋₄₉₈₀	5260 ⁺⁶⁸²⁰ ₋₂₉₇₀	-	9260 ⁺²⁷⁶⁰ ₋₂₁₉₀	8270 ⁺⁴⁴⁸⁰ ₋₄₂₂₀	8430 ± 1440	[80]
Hen 2-86	11550 ⁺²⁰⁴⁹⁰ ₋₅₂₄₀	9010 ⁺¹²²⁰⁰ ₋₄₄₇₀	41590 ⁺³³¹⁸⁰ ₋₁₉₂₂₀	21620 ⁺⁶¹⁹⁰ ₋₃₉₈₀	36560 ⁺⁵³⁹⁰ ₋₅₄₇₀	24730 ± 10360	[80]
M 2-31	7560 ⁺⁶⁶¹⁰ ₋₃₅₀	4740 ⁺²¹⁵⁰ ₋₁₃₃₀	-	9990 ⁺³⁷⁹⁰ ₋₃₂₉₀	8080 ⁺¹⁶⁷⁰ ₋₁₅₁₀	6940 ± 1830	[82]
NGC 5189	1270 ⁺³⁸⁰ ₋₃₅₀	1000 ⁺⁴⁵⁰ ₋₃₈₀	-	1370 ⁺⁵⁵⁰ ₋₅₆₀	1240 ⁺⁶⁵⁰ ₋₆₁₀	1130 ⁺⁴¹⁰ ₋₃₇₀	[80]
M 1-60	10590 ⁺¹⁵¹⁰⁰ ₋₅₈₈₀	6170 ⁺¹⁹⁰⁰ ₋₁₀₀₀	-	14110 ⁺⁸⁶⁵⁰ ₋₅₇₀₀	18230 ⁺²⁶⁶⁰ ₋₃₅₈₀	11210 ± 5650	[82]
Hen 2-73	9100 ⁺³⁰¹⁰ ₋₂₃₉₇₀	6510 ⁺⁴⁵¹⁰ ₋₂₂₆₀	-	12660 ⁺⁴⁶²⁰ ₋₃₅₄₀	-	9040 ± 2610	[82]
IC 4776	14320 ⁺⁷³⁸⁰ ₋₁₁₇₃₀	11380 ⁺⁴⁴⁰⁰ ₋₁₁₇₃₀	19480 ⁺²⁷¹²⁰ ₋₁₀₀₁₀	23470 ⁺⁶⁵⁹⁰ ₋₆₇₇₀	36820 ⁺³¹⁶⁰ ₋₃₄₈₀	29950 ± 9850	[84]
M 1-25	12300 ⁺⁵²¹⁰ ₋₃₃₀₀	6970 ⁺³⁶⁹⁰ ₋₁₇₅₀	11010 ⁺²⁰⁴³⁰ ₋₅₅₃₀₀	13690 ⁺²⁹⁰⁰ ₋₂₂₅₀	-	12930 ± 1980	[80]
M 1-33	5550 ⁺¹³⁹⁰ ₋₄₉₀	4370 ⁺¹²⁵⁰ ₋₇₃₀	14960 ⁺¹³⁴³⁰ ₋₁₁₃₀	7230 ⁺²⁶⁵⁰ ₋₂₃₇₀	-	5230 ± 1160	[82]
M 2-36	3900 ⁺⁴⁵⁰ ₋₁₀₆₀	2660 ⁺³⁰⁰ ₋₄₀₀	-	5190 ⁺¹¹³⁰ ₋₁₂₀₀	3960 ⁺⁹³⁰ ₋₈₇₀	3140 ± 710	[85]
Abell 46	3210 ⁺¹⁰⁸⁰ ₋₇₁₀	440 ⁺⁴⁰⁰ ₋₃₁₀	-	-	1370 ⁺⁷³⁰ ₋₈₉₀	1820 ⁺⁷³⁰ ₋₅₁₀	[52]

- discrepancy and chemical evolution. *MNRAS* **467**(3), 3759–3774 (2017) [arXiv:1702.01120](https://arxiv.org/abs/1702.01120) [astro-ph.GA]. <https://doi.org/10.1093/mnras/stx328>
- [17] Stasińska, G.: The interest of high spatial resolution observations of presumed metal-rich H II regions. *A&A* **85**(3), 359–361 (1980)
- [18] Garnett, D.R.: Electron Temperature Variations and the Measurement of Nebular Abundances. *AJ* **103**, 1330 (1992). <https://doi.org/10.1086/116146>
- [19] Esteban, C., Mesa-Delgado, A., Morisset, C., García-Rojas, J.: The chemical composition of Galactic ring nebulae around massive stars. *MNRAS* **460**(4), 4038–4062 (2016) [arXiv:1605.07800](https://arxiv.org/abs/1605.07800) [astro-ph.SR]. <https://doi.org/10.1093/mnras/stw1243>
- [20] Sota, A., Maíz Apellániz, J., Walborn, N.R., Alfaro, E.J., Barbá, R.H., Morrell, N.I., Gamén, R.C., Arias, J.I.: The Galactic O-Star Spectroscopic Survey. I. Classification System and Bright Northern Stars in the Blue-violet at $R \sim 2500$. *ApJS* **193**(2), 24 (2011) [arXiv:1101.4002](https://arxiv.org/abs/1101.4002) [astro-ph.GA]. <https://doi.org/10.1088/0067-0049/193/2/24>
- [21] Perez, E.: Temperature fluctuations and starburst evolution. *MNRAS* **290**(3), 465–470 (1997). <https://doi.org/10.1093/mnras/290.3.465>
- [22] Ercolano, B., Bastian, N., Stasińska, G.: The effects of spatially distributed ionization sources on the temperature structure of H II regions. *MNRAS* **379**(3), 945–955 (2007) [arXiv:0705.2726](https://arxiv.org/abs/0705.2726) [astro-ph]. <https://doi.org/10.1111/j.1365-2966.2007.12002.x>
- [23] Maiolino, R., Mannucci, F.: De re metallica: the cosmic chemical evolution of galaxies. *A&ARv* **27**(1), 3 (2019) [arXiv:1811.09642](https://arxiv.org/abs/1811.09642) [astro-ph.GA]. <https://doi.org/10.1007/s00159-018-0112-2>
- [24] Arellano-Córdova, K.Z., Berg, D.A., Chisholm, J., Haro, P.A., Dickinson, M., Finkelstein, S.L., Leclercq, F., Rogers, N.S.J., Simons, R.C., Skillman, E.D., Trump, J.R., Kartaltepe, J.S.: A First Look at the Abundance Pattern-O/H, C/O, and Ne/O-in $z \lesssim 7$ Galaxies with JWST/NIRSpec. *ApJ* **940**(1), 23 (2022) [arXiv:2208.02562](https://arxiv.org/abs/2208.02562) [astro-ph.GA]. <https://doi.org/10.3847/2041-8213/ac9ab2>
- [25] Curti, M., D’Eugenio, F., Carniani, S., Maiolino, R., Sandles, L., Witstok, J., Baker, W.M., Bennett, J.S., Piotrowska, J.M., Tacchella, S., Charlot, S., Nakajima, K., Maheson, G., Mannucci, F., Amiri, A., Arribas, S., Belfiore, F., Bonaventura, N.R., Bunker, A.J., Chevallard, J., Cresci, G., Curtis-Lake, E., Hayden-Pawson, C., Jones, G.C., Kumari, N., Laseter, I., Looser, T.J., Marconi, A., Maseda, M.V., Scholtz, J., Smit, R., Übler, H., Wallace, I.E.B.: The chemical enrichment in the early Universe as

- probed by JWST via direct metallicity measurements at $z \approx 8$. *MNRAS* **518**(1), 425–438 (2023) [arXiv:2207.12375](https://arxiv.org/abs/2207.12375) [astro-ph.GA]. <https://doi.org/10.1093/mnras/stac2737>
- [26] Katz, H., Saxena, A., Cameron, A.J., Carniani, S., Bunker, A.J., Arribas, S., Bhatawdekar, R., Bowler, R.A.A., Boyett, K.N.K., Cresci, G., Curtis-Lake, E., D'Eugenio, F., Kumari, N., Looser, T.J., Maiolino, R., Übler, H., Willott, C., Witstok, J.: First insights into the ISM at $z \approx 8$ with JWST: possible physical implications of a high [O III] $\lambda 4363$ /[O III] $\lambda 5007$. *MNRAS* **518**(1), 592–603 (2023) [arXiv:2207.13693](https://arxiv.org/abs/2207.13693) [astro-ph.GA]. <https://doi.org/10.1093/mnras/stac2657>
- [27] Luridiana, V., Morisset, C., Shaw, R.A.: PyNeb: a new tool for analyzing emission lines. I. Code description and validation of results. *A&A* **573**, 42 (2015) [arXiv:1410.6662](https://arxiv.org/abs/1410.6662) [astro-ph.IM]. <https://doi.org/10.1051/0004-6361/201323152>
- [28] Irimia, A., Froese Fischer, C.: Breit Pauli Oscillator Strengths, Lifetimes and Einstein A Coefficients in Singly Ionized Sulphur. *Phys. Scr.* **71**(2), 172–184 (2005). <https://doi.org/10.1238/Physica.Regular.071a00172>
- [29] Tayal, S.S., Zatsarinny, O.: Breit-Pauli Transition Probabilities and Electron Excitation Collision Strengths for Singly Ionized Sulfur. *ApJS* **188**, 32–45 (2010). <https://doi.org/10.1088/0067-0049/188/1/32>
- [30] Froese Fischer, C., Tachiev, G.: Breit-Pauli energy levels, lifetimes, and transition probabilities for the beryllium-like to neon-like sequences. *Atomic Data and Nuclear Data Tables* **87**, 1–184 (2004). <https://doi.org/10.1016/j.adt.2004.02.001>
- [31] Kisielius, R., Storey, P.J., Ferland, G.J., Keenan, F.P.: Electron-impact excitation of OII fine-structure levels. *MNRAS* **397**(2), 903–912 (2009) [arXiv:0907.4209](https://arxiv.org/abs/0907.4209) [astro-ph.IM]. <https://doi.org/10.1111/j.1365-2966.2009.14989.x>
- [32] Fritzsche, S., Fricke, B., Geschke, D., Heitmann, A., Sienkiewicz, J.E.: Forbidden Transitions in the Ground-State Configuration of Low-Z Phosphorus-like Ions. *ApJ* **518**(2), 994–1001 (1999). <https://doi.org/10.1086/307328>
- [33] Butler, K., Zeippen, C.J.: Effective collision strengths for fine-structure forbidden transitions in the $3p^3$ configuration of Cl(III). *A&A* **208**(1-2), 337–344 (1989)
- [34] Mendoza, C., Zeippen, C.J.: Transition probabilities for forbidden lines in the $3p^3$ configuration. *MNRAS* **198**, 127–139 (1982). <https://doi.org/10.1093/mnras/198.1.127>

- [35] Ramsbottom, C.A., Bell, K.L.: Effective Collision Strengths for Electron-Impact Excitation of Triply Ionized Argon. *Atomic Data and Nuclear Data Tables* **66**, 65 (1997). <https://doi.org/10.1006/adnd.1997.0741>
- [36] Quinet, P.: Transition probabilities for forbidden lines of Fe III. *A&AS* **116**, 573–578 (1996)
- [37] Zhang, H.: Atomic data from the Iron Project. XVIII. Electron impact excitation collision strengths and rate coefficients for Fe III. *A&AS* **119**, 523–528 (1996)
- [38] Domínguez-Guzmán, G., Rodríguez, M., García-Rojas, J., Esteban, C., Toribio San Cipriano, L.: The homogeneity of chemical abundances in H II regions of the Magellanic Clouds. *MNRAS* **517**(3), 4497–4514 (2022) [arXiv:2210.07460](https://arxiv.org/abs/2210.07460) [astro-ph.GA]. <https://doi.org/10.1093/mnras/stac2974>
- [39] Zhang, Y., Ercolano, B., Liu, X.-W.: Temperature fluctuations in H II regions: $t^{\hat{2}}$ for the two-phase model. *A&A* **464**(2), 631–634 (2007) [arXiv:astro-ph/0701139](https://arxiv.org/abs/astro-ph/0701139) [astro-ph]. <https://doi.org/10.1051/0004-6361:20066564>
- [40] Ferland, G.J., Henney, W.J., O’Dell, C.R., Peimbert, M.: The abundance discrepancy factor and $t^{\hat{2}}$ in nebulae: are non-thermal electrons the culprits? *Rev. Mex. Astron. Astrofis.* **52**, 261 (2016) [arXiv:1605.03634](https://arxiv.org/abs/1605.03634) [astro-ph.SR]
- [41] Peimbert, M., Peimbert, A., Ruiz, M.T.: The Chemical Composition of the Small Magellanic Cloud H II Region NGC 346 and the Primordial Helium Abundance. *ApJ* **541**(2), 688–700 (2000) [arXiv:astro-ph/0003154](https://arxiv.org/abs/astro-ph/0003154) [astro-ph]. <https://doi.org/10.1086/309485>
- [42] Esteban, C., Peimbert, M., García-Rojas, J., Ruiz, M.T., Peimbert, A., Rodríguez, M.: A reappraisal of the chemical composition of the Orion nebula based on Very Large Telescope echelle spectrophotometry. *MNRAS* **355**(1), 229–247 (2004) [arXiv:astro-ph/0408249](https://arxiv.org/abs/astro-ph/0408249) [astro-ph]. <https://doi.org/10.1111/j.1365-2966.2004.08313.x>
- [43] García-Rojas, J., Esteban, C., Peimbert, M., Costado, M.T., Rodríguez, M., Peimbert, A., Ruiz, M.T.: Faint emission lines in the Galactic HII regions M16, M20 and NGC 3603*. *MNRAS* **368**(1), 253–279 (2006) [arXiv:astro-ph/0601595](https://arxiv.org/abs/astro-ph/0601595) [astro-ph]. <https://doi.org/10.1111/j.1365-2966.2006.10105.x>
- [44] García-Rojas, J., Esteban, C., Peimbert, A., Rodríguez, M., Peimbert, M., Ruiz, M.T.: The chemical composition of the Galactic H II regions M8 and M17. A revision based on deep VLT echelle spectrophotometry. *Rev.*

- Mex. Astron. Astrofis. **43**, 3–31 (2007) [arXiv:astro-ph/0610065](https://arxiv.org/abs/astro-ph/0610065) [astro-ph]
- [45] Mesa-Delgado, A., Esteban, C., García-Rojas, J.: Small-Scale Behavior of the Physical Conditions and the Abundance Discrepancy in the Orion Nebula. *ApJ* **675**(1), 389–404 (2008) [arXiv:0710.1285](https://arxiv.org/abs/0710.1285) [astro-ph]. <https://doi.org/10.1086/524296>
- [46] Méndez-Delgado, J.E., Henney, W.J., Esteban, C., García-Rojas, J., Mesa-Delgado, A., Arellano-Córdova, K.Z.: Photoionized Herbig-Haro Objects in the Orion Nebula through Deep High Spectral Resolution Spectroscopy. II. HH 204. *ApJ* **918**(1), 27 (2021) [arXiv:2106.08667](https://arxiv.org/abs/2106.08667) [astro-ph.GA]. <https://doi.org/10.3847/1538-4357/ac0cf5>
- [47] Liu, X.-W., Luo, S.-G., Barlow, M.J., Danziger, I.J., Storey, P.J.: Chemical abundances of planetary nebulae from optical recombination lines - III. The Galactic bulge PN M 1-42 and M 2-36. *MNRAS* **327**(1), 141–168 (2001). <https://doi.org/10.1046/j.1365-8711.2001.04676.x>
- [48] Wesson, R., Liu, X.-W., Barlow, M.J.: Physical conditions in the planetary nebula Abell 30. *MNRAS* **340**(1), 253–263 (2003) [arXiv:astro-ph/0301119](https://arxiv.org/abs/astro-ph/0301119) [astro-ph]. <https://doi.org/10.1046/j.1365-8711.2003.06289.x>
- [49] Liu, X.-W., Barlow, M.J., Zhang, Y., Bastin, R.J., Storey, P.J.: Chemical abundances for Hf 2-2, a planetary nebula with the strongest-known heavy-element recombination lines. *MNRAS* **368**(4), 1959–1970 (2006) [arXiv:astro-ph/0603215](https://arxiv.org/abs/astro-ph/0603215) [astro-ph]. <https://doi.org/10.1111/j.1365-2966.2006.10283.x>
- [50] Storey, P.J., Sochi, T.: The continuum emission spectrum of Hf 2-2 near the Balmer limit and the ORL versus CEL abundance and temperature discrepancy. *MNRAS* **440**(3), 2581–2587 (2014) [arXiv:1401.5630](https://arxiv.org/abs/1401.5630) [astro-ph.SR]. <https://doi.org/10.1093/mnras/stu477>
- [51] García-Rojas, J., Morisset, C., Jones, D., Wesson, R., Boffin, H.M.J., Monteiro, H., Corradi, R.L.M., Rodríguez-Gil, P.: MUSE spectroscopy of planetary nebulae with high abundance discrepancies. *MNRAS* **510**(4), 5444–5463 (2022) [arXiv:2112.00480](https://arxiv.org/abs/2112.00480) [astro-ph.SR]. <https://doi.org/10.1093/mnras/stab3523>
- [52] Corradi, R.L.M., García-Rojas, J., Jones, D., Rodríguez-Gil, P.: Bina- rity and the Abundance Discrepancy Problem in Planetary Nebulae. *ApJ* **803**(2), 99 (2015) [arXiv:1502.05182](https://arxiv.org/abs/1502.05182) [astro-ph.SR]. <https://doi.org/10.1088/0004-637X/803/2/99>
- [53] Richer, M.G., Arrieta, A., Arias, L., Castañeda-Carlos, L., Torres- Peimbert, S., López, J.A., Galindo, A.: NGC 6153: Reality is Complicated. *AJ* **164**(6), 243 (2022) [arXiv:2210.05085](https://arxiv.org/abs/2210.05085) [astro-ph.GA]. <https://doi.org/>

[10.3847/1538-3881/ac9732](https://doi.org/10.3847/1538-3881/ac9732)

- [54] Storey, P.J., Hummer, D.G.: Recombination line intensities for hydrogenic ions-IV. Total recombination coefficients and machine-readable tables for $Z=1$ to 8. *MNRAS* **272**(1), 41–48 (1995). <https://doi.org/10.1093/mnras/272.1.41>
- [55] Wiese, W.L., Fuhr, J.R., Deters, T.M.: Atomic transition probabilities of carbon, nitrogen, and oxygen : a critical data compilation. *Journal of Physical and Chemical Reference Data, Monograph 7* **403** (1996)
- [56] Storey, P.J., Zeippen, C.J.: Theoretical values for the [Oiii] 5007/4959 line-intensity ratio and homologous cases. *MNRAS* **312**, 813–816 (2000). <https://doi.org/10.1046/j.1365-8711.2000.03184.x>
- [57] Storey, P.J., Sochi, T., Badnell, N.R.: Collision strengths for nebular [O III] optical and infrared lines. *MNRAS* **441**, 3028–3039 (2014). <https://doi.org/10.1093/mnras/stu777>
- [58] Tayal, S.S.: Electron Excitation Collision Strengths for Singly Ionized Nitrogen. *ApJS* **195**, 12 (2011). <https://doi.org/10.1088/0067-0049/195/2/12>
- [59] Mendoza, C.: Recent advances in atomic calculations and experiments of interest in the study of planetary nebulae. In: Aller, L.H. (ed.) *Planetary Nebulae*. IAU Symposium, vol. 103, pp. 143–172 (1983)
- [60] Kaufman, V., Sugar, J.: Forbidden Lines in ns^2np^k Ground Configurations and $nsnp$ Excited Configurations of Beryllium through Molybdenum Atoms and Ions. *Journal of Physical and Chemical Reference Data* **15**(1), 321–426 (1986). <https://doi.org/10.1063/1.555775>
- [61] Galavis, M.E., Mendoza, C., Zeippen, C.J.: Atomic data from the IRON Project. X. Effective collision strengths for infrared transitions in silicon- and sulphur-like ions. *A&AS* **111**, 347 (1995)
- [62] Esteban, C., Bresolin, F., Peimbert, M., García-Rojas, J., Peimbert, A., Mesa-Delgado, A.: Keck HIRES Spectroscopy of Extragalactic H II Regions: C and O Abundances from Recombination Lines. *ApJ* **700**(1), 654–678 (2009) [arXiv:0905.2532](https://arxiv.org/abs/0905.2532) [astro-ph.CO]. <https://doi.org/10.1088/0004-637X/700/1/654>
- [63] Toribio San Cipriano, L., García-Rojas, J., Esteban, C., Bresolin, F., Peimbert, M.: Carbon and oxygen abundance gradients in NGC 300 and M33 from optical recombination lines. *MNRAS* **458**(2), 1866–1890 (2016) [arXiv:1602.05587](https://arxiv.org/abs/1602.05587) [astro-ph.GA]. <https://doi.org/10.1093/mnras/stw397>

- [64] Esteban, C., Bresolin, F., García-Rojas, J., Toribio San Cipriano, L.: Carbon, nitrogen, and oxygen abundance gradients in M101 and M31. *MNRAS* **491**(2), 2137–2155 (2020) [arXiv:1911.01981](https://arxiv.org/abs/1911.01981) [astro-ph.GA]. <https://doi.org/10.1093/mnras/stz3134>
- [65] Esteban, C., García-Rojas, J., Carigi, L., Peimbert, M., Bresolin, F., López-Sánchez, A.R., Mesa-Delgado, A.: Carbon and oxygen abundances from recombination lines in low-metallicity star-forming galaxies. Implications for chemical evolution. *MNRAS* **443**(1), 624–647 (2014) [arXiv:1406.3986](https://arxiv.org/abs/1406.3986) [astro-ph.GA]. <https://doi.org/10.1093/mnras/stu1177>
- [66] López-Sánchez, Á.R., Esteban, C., García-Rojas, J., Peimbert, M., Rodríguez, M.: The Localized Chemical Pollution in NGC 5253 Revisited: Results from Deep Echelle Spectrophotometry. *ApJ* **656**(1), 168–185 (2007) [arXiv:astro-ph/0609498](https://arxiv.org/abs/astro-ph/0609498) [astro-ph]. <https://doi.org/10.1086/510112>
- [67] Peimbert, A.: The Chemical Composition of the 30 Doradus Nebula Derived from Very Large Telescope Echelle Spectrophotometry. *ApJ* **584**(2), 735–750 (2003) [arXiv:astro-ph/0208502](https://arxiv.org/abs/astro-ph/0208502) [astro-ph]. <https://doi.org/10.1086/345793>
- [68] Guseva, N.G., Izotov, Y.I., Stasińska, G., Fricke, K.J., Henkel, C., Papaderos, P.: VLT spectroscopy of low-metallicity emission-line galaxies: abundance patterns and abundance discrepancies. *A&A* **529**, 149 (2011) [arXiv:1111.1392](https://arxiv.org/abs/1111.1392) [astro-ph.CO]. <https://doi.org/10.1051/0004-6361/201016291>
- [69] Peimbert, A., Peimbert, M., Ruiz, M.T.: Chemical Composition of Two H II Regions in NGC 6822 Based on VLT Spectroscopy. *ApJ* **634**(2), 1056–1066 (2005) [arXiv:astro-ph/0507084](https://arxiv.org/abs/astro-ph/0507084) [astro-ph]. <https://doi.org/10.1086/444557>
- [70] Valerdi, M., Peimbert, A., Peimbert, M., Sixtos, A.: Determination of the Primordial Helium Abundance Based on NGC 346, an H II Region of the Small Magellanic Cloud. *ApJ* **876**(2), 98 (2019) [arXiv:1904.01594](https://arxiv.org/abs/1904.01594) [astro-ph.GA]. <https://doi.org/10.3847/1538-4357/ab14e4>
- [71] Peña-Guerrero, M.A., Peimbert, A., Peimbert, M., Ruiz, M.T.: Analysis of Two Small Magellanic Cloud H II Regions Considering Thermal Inhomogeneities: Implications for the Determinations of Extragalactic Chemical Abundances. *ApJ* **746**(2), 115 (2012) [arXiv:1111.2844](https://arxiv.org/abs/1111.2844) [astro-ph.CO]. <https://doi.org/10.1088/0004-637X/746/2/115>
- [72] Delgado-Inglada, G., Mesa-Delgado, A., García-Rojas, J., Rodríguez, M., Esteban, C.: The Fe/Ni ratio in ionized nebulae: clues on dust depletion patterns. *MNRAS* **456**(4), 3855–3865 (2016) [arXiv:1512.05664](https://arxiv.org/abs/1512.05664)

- [astro-ph.SR]. <https://doi.org/10.1093/mnras/stv2961>
- [73] Méndez-Delgado, J.E., Esteban, C., García-Rojas, J., Henney, W.J.: Photoionized Herbig-Haro objects in the Orion Nebula through deep high-spectral resolution spectroscopy - III. HH 514. *MNRAS* **514**(1), 744–761 (2022) [arXiv:2205.03266](https://arxiv.org/abs/2205.03266) [astro-ph.GA]. <https://doi.org/10.1093/mnras/stac1300>
- [74] Esteban, C., Fang, X., García-Rojas, J., Toribio San Cipriano, L.: The radial abundance gradient of oxygen towards the Galactic anti-centre. *MNRAS* **471**(1), 987–1004 (2017) [arXiv:1706.07727](https://arxiv.org/abs/1706.07727) [astro-ph.GA]. <https://doi.org/10.1093/mnras/stx1624>
- [75] Méndez-Delgado, J.E., Esteban, C., García-Rojas, J., Henney, W.J., Mesa-Delgado, A., Arellano-Córdova, K.Z.: Photoionized Herbig-Haro objects in the Orion Nebula through deep high-spectral resolution spectroscopy - I. HH 529 II and III. *MNRAS* **502**(2), 1703–1739 (2021) [arXiv:2101.02191](https://arxiv.org/abs/2101.02191) [astro-ph.GA]. <https://doi.org/10.1093/mnras/stab068>
- [76] García-Rojas, J., Esteban, C., Peimbert, A., Peimbert, M., Rodríguez, M., Ruiz, M.T.: Deep echelle spectrophotometry of S 311, a Galactic H II region located outside the solar circle. *MNRAS* **362**(1), 301–312 (2005) [arXiv:astro-ph/0506409](https://arxiv.org/abs/astro-ph/0506409) [astro-ph]. <https://doi.org/10.1111/j.1365-2966.2005.09302.x>
- [77] García-Rojas, J., Esteban, C., Peimbert, M., Rodríguez, M., Ruiz, M.T., Peimbert, A.: Chemical Abundances of the Galactic H II Region NGC 3576 Derived from Very Large Telescope Echelle Spectrophotometry. *ApJS* **153**(2), 501–522 (2004) [arXiv:astro-ph/0404123](https://arxiv.org/abs/astro-ph/0404123) [astro-ph]. <https://doi.org/10.1086/421909>
- [78] Mesa-Delgado, A., Esteban, C., García-Rojas, J., Luridiana, V., Bautista, M., Rodríguez, M., López-Martín, L., Peimbert, M.: Properties of the ionized gas in HH 202 - II. Results from echelle spectrophotometry with Ultraviolet Visual Echelle Spectrograph. *MNRAS* **395**(2), 855–876 (2009) [arXiv:0901.4311](https://arxiv.org/abs/0901.4311) [astro-ph.GA]. <https://doi.org/10.1111/j.1365-2966.2009.14554.x>
- [79] Sharpee, B., Zhang, Y., Williams, R., Pellegrini, E., Cavagnolo, K., Baldwin, J.A., Phillips, M., Liu, X.-W.: s-Process Abundances in Planetary Nebulae. *ApJ* **659**(2), 1265–1290 (2007) [arXiv:astro-ph/0612101](https://arxiv.org/abs/astro-ph/0612101) [astro-ph]. <https://doi.org/10.1086/511665>
- [80] García-Rojas, J., Peña, M., Morisset, C., Mesa-Delgado, A., Ruiz, M.T.: Analysis of chemical abundances in planetary nebulae with [WC] central stars. I. Line intensities and physical conditions. *A&A* **538**, 54 (2012) [arXiv:1111.4992](https://arxiv.org/abs/1111.4992) [astro-ph.GA]. <https://doi.org/10.1051/>

0004-6361/201118217

- [81] Madonna, S., García-Rojas, J., Sterling, N.C., Delgado-Inglada, G., Mesa-Delgado, A., Luridiana, V., Roederer, I.U., Mashburn, A.L.: Neutron-capture element abundances in the planetary nebula NGC 5315 from deep optical and near-infrared spectrophotometry†. *MNRAS* **471**(2), 1341–1369 (2017) [arXiv:1706.07225](https://arxiv.org/abs/1706.07225) [astro-ph.SR]. <https://doi.org/10.1093/mnras/stx1585>
- [82] García-Rojas, J., Delgado-Inglada, G., García-Hernández, D.A., Dell’Agli, F., Lugaro, M., Karakas, A.I., Rodríguez, M.: C/O ratios in planetary nebulae with dual-dust chemistry from faint optical recombination lines. *MNRAS* **473**(4), 4476–4496 (2018) [arXiv:1709.07958](https://arxiv.org/abs/1709.07958) [astro-ph.SR]. <https://doi.org/10.1093/mnras/stx2519>
- [83] Sharpee, B., Williams, R., Baldwin, J.A., van Hoof, P.A.M.: Introducing EMILI: Computer-aided Emission Line Identification. *ApJS* **149**(1), 157–187 (2003) [arXiv:astro-ph/0307053](https://arxiv.org/abs/astro-ph/0307053) [astro-ph]. <https://doi.org/10.1086/378321>
- [84] Sowicka, P., Jones, D., Corradi, R.L.M., Wesson, R., García-Rojas, J., Santander-García, M., Boffin, H.M.J., Rodríguez-Gil, P.: The planetary nebula IC 4776 and its post-common-envelope binary central star. *MNRAS* **471**(3), 3529–3546 (2017) [arXiv:1706.08766](https://arxiv.org/abs/1706.08766) [astro-ph.SR]. <https://doi.org/10.1093/mnras/stx1697>
- [85] Espíritu, J.N., Peimbert, A.: Physical conditions and chemical abundances in PN M 2-36. Results from deep echelle observations. *MNRAS* **508**(2), 2668–2687 (2021) [arXiv:2109.10546](https://arxiv.org/abs/2109.10546) [astro-ph.GA]. <https://doi.org/10.1093/mnras/stab2746>

Table A6 Electron temperature values of the adopted sample of Galactic H II regions and planetary nebulae.

Region	$T_e(\text{[O III]})$ K	$T_e(\text{[Ar III]})$ K	$T_e(\text{[N II]})$ K	Ref.
Galactic H II regions				
NGC 3603	9020 ⁺¹³⁰ ₋₁₂₀	-	11040 ⁺⁶⁵⁰ ₋₅₃₀	[43]
M 42-P1	8320 ⁺⁸⁰ ₋₆₀	7970 ± 440	9500 ⁺²⁵⁰ ₋₂₆₀	[72]
M 42-2	8500 ⁺⁶⁰ ₋₇₀	8100 ⁺¹³⁰ ₋₁₅₀	9810 ⁺²³⁰ ₋₂₀₀	[73]
Sh 2-100	8280 ⁺¹⁰⁰ ₋₁₂₀	7650 ⁺³⁸⁰ ₋₅₂₀	8430 ⁺²⁷⁰ ₋₃₀₀	[74]
M 42-3	8510 ± 60	8260 ⁺¹⁶⁰ ₋₂₀₀	10090 ⁺²³⁰ ₋₂₀₀	[75]
M 42-1	8420 ⁺⁸⁰ ₋₆₀	8270 ⁺²¹⁰ ₋₂₂₀	9920 ⁺²¹⁰ ₋₂₀₀	[75]
Sh 2-311	8960 ⁺⁹⁰ ₋₁₀₀	8830 ⁺⁸⁹⁰ ₋₉₅₀	9230 ⁺¹⁷⁰ ₋₂₄₀	[76]
M 16	7600 ⁺¹⁴⁰ ₋₁₃₀	-	8280 ⁺²³⁰ ₋₁₃₀	[43]
M 42-bar	8470 ⁺⁹⁰ ₋₇₀	8330 ⁺³²⁰ ₋₂₉₀	9000 ⁺¹³⁰ ₋₁₅₀	[72]
M 42-1	8020 ⁺⁶⁰ ₋₅₀	-	8510 ⁺¹⁴⁰ ₋₁₁₀	[46]
NGC 3576	8450 ⁺⁴⁰ ₋₅₀	8590 ⁺³⁴⁰ ₋₂₇₀	8710 ⁺¹⁶⁰ ₋₂₇₀	[77]
M 42	8380 ± 60	8190 ⁺²⁵⁰ ₋₃₆₀	9920 ⁺²⁹⁰ ₋₂₂₀	[42]
M 17	7950 ⁺¹⁰⁰ ₋₉₀	8350 ⁺⁴⁸⁰ ₋₅₁₀	8740 ⁺²²⁰ ₋₁₈₀	[44]
M 8	8050 ⁺¹¹⁰ ₋₁₀₀	7570 ± 310	8330 ± 100	[44]
M 42-4	8320 ⁺⁹⁰ ₋₆₀	8250 ⁺³²⁰ ₋₃₆₀	9890 ⁺²²⁰ ₋₂₁₀	[75]
M 42-3	8410 ⁺⁵⁰ ₋₆₀	8310 ± 200	9890 ⁺¹⁹⁰ ₋₂₆₀	[73]
Sh 2-288	9260 ⁺⁵²⁰ ₋₆₂₀	-	9390 ⁺³⁴⁰ ₋₃₅₀	[74]
M 42	8180 ⁺¹⁴⁰ ₋₂₆₀	7880 ⁺⁴⁶⁰ ₋₅₂₀	9430 ⁺³⁸⁰ ₋₃₂₀	[78]
M 42-2	8120 ⁺⁵⁰ ₋₇₀	-	8450 ⁺¹⁴⁰ ₋₁₅₀	[46]
M 42-2	8390 ⁺⁷⁰ ₋₅₀	8330 ⁺¹⁸⁰ ₋₁₃₀	9860 ⁺²³⁰ ₋₁₇₀	[75]
Galactic planetary nebulae				
NGC 2440	14850 ⁺²⁹⁰ ₋₃₀₀	12120 ± 260	13880 ⁺⁴⁷⁰ ₋₄₅₀	[79]
Hb 4	10010 ⁺²⁶⁰ ₋₂₀₀	8290 ⁺⁵⁵⁰ ₋₄₀₀	9810 ⁺⁴⁴⁰ ₋₆₉₀	[80]
NGC 5315	8760 ⁺²²⁰ ₋₂₅₀	8330 ⁺²⁸⁰ ₋₃₂₀	10060 ⁺¹³⁰ ₋₇₈₀	[81]
M 1-31	8310 ⁺¹⁸⁰ ₋₂₄₀	-	10210 ⁺⁴¹⁰ ₋₅₃₀	[82]
Cn 1-5	8740 ± 180	7840 ⁺³²⁰ ₋₃₃₀	8710 ⁺³⁴⁰ ₋₂₁₀	[80]
H 1-40	10100 ⁺³⁹⁰ ₋₃₇₀	-	13850 ⁺⁶⁷⁰ ₋₁₁₄₀	[82]
H 1-50	11090 ± 230	10480 ± 820	11840 ⁺⁵¹⁰ ₋₅₂₀	[82]
Hen 2-158	9280 ⁺¹⁸⁰ ₋₂₂₀	-	10100 ± 350	[82]
IC 418	8770 ⁺⁹⁰ ₋₁₀₀	8600 ⁺³⁸⁰ ₋₃₀₀	9340 ⁺²⁸⁰ ₋₂₁₀	[83]
PC 14	9270 ⁺²¹⁰ ₋₁₇₀	8830 ⁺⁴⁴⁰ ₋₅₅₀	10220 ± 430	[80]
M 1-32	9370 ⁺²⁴⁰ ₋₂₁₀	8040 ⁺⁶²⁰ ₋₈₀₀	8920 ⁺⁴³⁰ ₋₄₉₀	[80]
M 1-61	9190 ⁺²⁴⁰ ₋₂₄₀	8730 ⁺³⁸⁰ ₋₃₇₀	12680 ⁺¹³¹⁰ ₋₈₇₀	[80]
Ou5	12470 ⁺⁴⁴⁰ ₋₃₈₀	-	25870 ⁺⁹⁹⁴⁰ ₋₆₄₂₀	[52]
NGC 6369	10650 ⁺³³⁰ ₋₂₄₀	9280 ⁺⁸⁰⁰ ₋₉₂₀	13320 ⁺⁵⁷⁰ ₋₆₇₀	[80]
Pe 1-1	10100 ⁺³⁴⁰ ₋₂₉₀	9220 ⁺⁵⁵⁰ ₋₄₉₀	12250 ⁺¹⁰¹⁰ ₋₁₀₈₀	[80]
IC 2501	9410 ⁺⁸⁰ ₋₁₁₀	8840 ⁺³²⁰ ₋₂₅₀	10930 ⁺²³⁰ ₋₂₁₀	[79]
M 1-30	6640 ⁺⁸⁰ ₋₁₇₀	6430 ⁺¹⁸⁰ ₋₂₅₀	6990 ⁺²⁶⁰ ₋₂₃₀	[80]
IC 4191	9740 ⁺¹⁴⁰ ₋₁₅₀	12000 ⁺²³⁰ ₋₁₃₀	12120 ⁺³⁷⁰ ₋₄₁₀	[79]
Hen 2-96	8990 ⁺¹⁷⁰ ₋₂₃₀	-	11540 ⁺⁸⁰⁰ ₋₈₃₀	[82]
M 3-15	8360 ⁺²⁵⁰ ₋₂₂₀	-	11210 ⁺⁶⁶⁰ ₋₇₃₀	[80]
Hen 2-86	8320 ± 210	9450 ± 370	10260 ⁺¹¹²⁰ ₋₇₈₀	[80]

Table A6 Continued.

Region	T_e ([O III]) K	T_e ([Ar III]) K	T_e ([N II]) K	Ref.
M 2-31	9900^{+270}_{-190}	-	11090^{+460}_{-430}	[82]
NGC 5189	11450^{+300}_{-280}	10310^{+460}_{-430}	9480^{+450}_{-320}	[80]
M 1-60	8800^{+210}_{-200}	-	9810^{+540}_{-560}	[82]
Hen 2-73	11770^{+380}_{-220}	9650^{+1060}_{-1040}	11480^{+460}_{-500}	[82]
IC 4776	9960^{+150}_{-210}	9230 ± 190	10110^{+860}_{-920}	[84]
M 1-25	7800 ± 170	-	8290^{+370}_{-280}	[80]
M 1-33	8930^{+170}_{-200}	-	9530^{+260}_{-270}	[82]
M 2-36	8390^{+120}_{-100}	7020^{+270}_{-590}	14350^{+270}_{-480}	[85]
Abell 46	12930^{+260}_{-280}	-	29300^{+18610}_{-9210}	[52]

Table A7 O II V1 fluxes and their associated physical parameters of the H II regions and other nebulae.

Region	$T_e(\text{O II}/[\text{O III}])$ K	$T_0(\text{O}^{2+})$ K	$t^2(\text{O}^{2+})$	O II V1/H β H β =100	No. lines	Ref.
Extragalactic H II regions						
NGC 5461	7640 \pm 880	7480 \pm 1080	0.027 \pm 0.030	0.387 \pm 0.123	2	[62]
NGC 588	9320 \pm 600	9330 \pm 740	0.044 \pm 0.025	0.281 \pm 0.057	5	[63]
NGC 595	6380 \pm 270	6240 \pm 430	0.031 \pm 0.015	0.290 \pm 0.057	2	[62]
K 932	7460 \pm 310	7350 \pm 370	0.026 \pm 0.011	0.415 \pm 0.070	5	[62]
IC 132	9340 \pm 730	9390 \pm 830	0.026 \pm 0.029	0.323 \pm 0.078	3	[63]
N 11B	8140 \pm 150	8060 \pm 170	0.031 \pm 0.006	0.307 \pm 0.023	5	[38]
NGC 5471	12700 \pm 2100	12890 \pm 2210	0.032 \pm 0.078	0.146 \pm 0.050	2	[64]
N 66A	11230 \pm 440	11330 \pm 450	0.041 \pm 0.015	0.128 \pm 0.015	1	[38]
NGC 604	7270 \pm 250	7170 \pm 320	0.025 \pm 0.010	0.354 \pm 0.055	5	[62]
NGC 6822	9740 \pm 510	9720 \pm 590	0.055 \pm 0.018	0.277 \pm 0.046	6	[65]
UV-1	8420 \pm 1080	8390 \pm 1410	0.071 \pm 0.037	0.398 \pm 0.126	2	[66]
NGC 5408	10610 \pm 900	10890 \pm 1170	0.162 \pm 0.032	0.207 \pm 0.044	6	[65]
NGC 1714	8470 \pm 410	8410 \pm 490	0.033 \pm 0.015	0.368 \pm 0.064	6	[38]
N 81	10100 \pm 180	10140 \pm 190	0.084 \pm 0.009	0.216 \pm 0.013	5	[38]
IC 2111	8300 \pm 530	8230 \pm 620	0.025 \pm 0.018	0.285 \pm 0.060	7	[38]
NGC 2363	12160 \pm 1330	12730 \pm 1550	0.129 \pm 0.048	0.142 \pm 0.035	5	[62]
30Dor	8970 \pm 270	8940 \pm 300	0.027 \pm 0.009	0.339 \pm 0.037	8	[67]
N 44C	9010 \pm 190	8930 \pm 230	0.070 \pm 0.007	0.483 \pm 0.039	6	[38]
HII-2	8470 \pm 1050	8130 \pm 1450	0.108 \pm 0.036	0.477 \pm 0.162	1	[66]
NGC 5455	9000 \pm 1360	9000 \pm 1520	0.018 \pm 0.045	0.251 \pm 0.083	3	[64]
VS44	7220 \pm 940	7050 \pm 1200	0.031 \pm 0.033	0.332 \pm 0.120	5	[62]
N 88A	11860 \pm 180	12060 \pm 190	0.060 \pm 0.010	0.183 \pm 0.008	5	[38]
HII-1	8540 \pm 1020	8360 \pm 1460	0.105 \pm 0.037	0.477 \pm 0.161	1	[66]
Galactic ring nebulae						
NGC 7635A2	6140 \pm 650	5810 \pm 970	0.060 \pm 0.028	0.888 \pm 0.262	3	[19]
NGC 7635A3	6280 \pm 430	6040 \pm 670	0.041 \pm 0.023	0.695 \pm 0.189	3	[19]
NGC 7635A4	7170 \pm 570	7020 \pm 780	0.045 \pm 0.022	0.104 \pm 0.027	2	[19]
NGC 6888A2	5060 \pm 170	2380 \pm 650	0.244 \pm 0.014	2.224 \pm 0.434	1	[19]
NGC 6888A3	5470 \pm 260	4280 \pm 680	0.145 \pm 0.022	0.983 \pm 0.229	3	[19]
NGC 6888A4	6770 \pm 770	6180 \pm 1330	0.104 \pm 0.039	0.577 \pm 0.169	4	[19]
NGC 6888A5	6470 \pm 410	5840 \pm 730	0.106 \pm 0.021	0.721 \pm 0.195	5	[19]
NGC 6888A6	6940 \pm 320	6520 \pm 580	0.084 \pm 0.024	0.488 \pm 0.097	3	[19]

Table A7 Continued.

Region	$T_e(\text{O II}/[\text{O III}])$ K	$T_0(\text{O}^{2+})$ K	$t^2(\text{O}^{2+})$	O II V1/H β H β =100	No. lines	Ref.
Galactic H II regions						
NGC 3603	7550 \pm 560	7410 \pm 720	0.046 \pm 0.019	0.644 \pm 0.167	4	[43]
M 42-P1	7580 \pm 230	7510 \pm 280	0.022 \pm 0.008	0.417 \pm 0.052	6	[72]
M 42-2	7390 \pm 60	7250 \pm 80	0.035 \pm 0.003	0.472 \pm 0.015	6	[73]
Sh 2-100	7380 \pm 320	7280 \pm 400	0.028 \pm 0.011	0.501 \pm 0.091	6	[74]
M 42-3	7660 \pm 120	7560 \pm 140	0.027 \pm 0.004	0.403 \pm 0.025	5	[75]
M 42-1	7730 \pm 130	7660 \pm 160	0.022 \pm 0.005	0.355 \pm 0.025	5	[75]
Sh 2-311	7770 \pm 900	7750 \pm 1120	0.035 \pm 0.031	0.152 \pm 0.048	5	[76]
M 16	6240 \pm 320	6010 \pm 420	0.042 \pm 0.011	0.252 \pm 0.058	5	[43]
M 42-bar	7620 \pm 260	7550 \pm 290	0.026 \pm 0.008	0.198 \pm 0.028	6	[72]
M 42-1	7170 \pm 110	7070 \pm 140	0.026 \pm 0.004	0.181 \pm 0.012	5	[46]
NGC 3576	7140 \pm 130	6960 \pm 160	0.041 \pm 0.004	0.559 \pm 0.043	6	[77]
M 42	7370 \pm 130	7250 \pm 160	0.031 \pm 0.005	0.499 \pm 0.038	6	[42]
M 17	6980 \pm 280	6870 \pm 340	0.029 \pm 0.009	0.638 \pm 0.108	6	[44]
M 8	6670 \pm 210	6470 \pm 280	0.043 \pm 0.008	0.210 \pm 0.030	6	[44]
M 42-4	7550 \pm 100	7470 \pm 120	0.024 \pm 0.004	0.403 \pm 0.021	5	[75]
M 42-3	7320 \pm 80	7200 \pm 100	0.033 \pm 0.003	0.498 \pm 0.022	6	[73]
Sh 2-288	7440 \pm 1080	7420 \pm 1520	0.053 \pm 0.042	0.170 \pm 0.062	2	[74]
M 42	7460 \pm 290	7380 \pm 360	0.022 \pm 0.011	0.394 \pm 0.061	6	[78]
M 42-2	6710 \pm 150	6480 \pm 180	0.044 \pm 0.005	0.305 \pm 0.030	4	[46]
M 42-2	7670 \pm 70	7600 \pm 90	0.022 \pm 0.003	0.382 \pm 0.012	6	[75]
Extragalactic H II regions from the literature						
NGC 456a-1	9360 \pm 780	9270 \pm 970	0.089 \pm 0.026	0.212 \pm 0.050	2	[68]
NGC 456a-2	8920 \pm 1020	8830 \pm 1330	0.092 \pm 0.035	0.294 \pm 0.095	2	[68]
NGC 6822V	10030 \pm 1090	10040 \pm 1240	0.051 \pm 0.037	0.249 \pm 0.071	4	[69]
NGC 5253C1	11820 \pm 720	11910 \pm 690	0.009 \pm 0.023	0.166 \pm 0.027	2	[68]
Mrk1259	5400 \pm 400	4220 \pm 760	0.143 \pm 0.018	1.160 \pm 0.333	2	[68]
NGC 5253C2	9290 \pm 590	9270 \pm 650	0.027 \pm 0.019	0.270 \pm 0.056	2	[68]
NGC 5253P2	10030 \pm 910	10000 \pm 1070	0.071 \pm 0.030	0.281 \pm 0.065	2	[68]
NGC 346	9840 \pm 530	9830 \pm 630	0.092 \pm 0.018	0.261 \pm 0.045	4	[70]
NGC 456-2	9940 \pm 1230	9970 \pm 1510	0.065 \pm 0.043	0.189 \pm 0.054	4	[71]

Table A7 Continued.

Region	$T_e(\text{O II}/[\text{O III}])$ K	$T_0(\text{O}^{2+})$ K	$t^2(\text{O}^{2+})$	O II V1/H β H β =100	No. lines	Ref.
Galactic planetary nebulae						
NGC 2440	11470 \pm 330	11750 \pm 370	0.104 \pm 0.014	0.394 \pm 0.031	4	[79]
Hb 4	7030 \pm 270	6600 \pm 400	0.093 \pm 0.012	1.808 \pm 0.282	4	[80]
NGC 5315	7530 \pm 230	7390 \pm 300	0.038 \pm 0.011	1.011 \pm 0.106	6	[81]
M 1-31	6970 \pm 550	6820 \pm 730	0.041 \pm 0.020	1.300 \pm 0.309	3	[82]
Cn 1-5	7370 \pm 450	7180 \pm 580	0.043 \pm 0.016	1.138 \pm 0.251	3	[80]
H 1-40	7600 \pm 1040	7360 \pm 1440	0.077 \pm 0.038	1.084 \pm 0.421	1	[82]
H 1-50	8290 \pm 390	8070 \pm 500	0.086 \pm 0.015	1.259 \pm 0.204	3	[82]
Hen 2158	8190 \pm 1010	8200 \pm 1220	0.032 \pm 0.034	0.441 \pm 0.159	2	[82]
IC 418	7910 \pm 230	7830 \pm 260	0.027 \pm 0.008	0.207 \pm 0.023	8	[83]
PC 14	7630 \pm 400	7460 \pm 510	0.050 \pm 0.014	1.362 \pm 0.264	3	[80]
M 1-32	7050 \pm 260	6710 \pm 390	0.072 \pm 0.011	0.691 \pm 0.105	2	[80]
M 1-61	7760 \pm 350	7620 \pm 440	0.045 \pm 0.013	0.946 \pm 0.162	5	[80]
Ou5	4380 \pm 130	1060 \pm 630	0.258 \pm 0.014	14.436 \pm 2.766	4	[52]
NGC 6369	9220 \pm 630	9180 \pm 690	0.044 \pm 0.022	0.624 \pm 0.133	3	[80]
Pe 1-1	8270 \pm 550	8130 \pm 700	0.057 \pm 0.020	0.815 \pm 0.187	4	[80]
IC 2501	9270 \pm 180	9260 \pm 190	0.005 \pm 0.006	0.463 \pm 0.030	8	[79]
M 1-30	5440 \pm 120	5180 \pm 190	0.038 \pm 0.006	1.032 \pm 0.116	5	[80]
IC 4191	8040 \pm 100	7900 \pm 130	0.052 \pm 0.005	1.460 \pm 0.062	8	[79]
Hen 2-96	8000 \pm 590	7890 \pm 710	0.032 \pm 0.020	0.780 \pm 0.184	5	[82]
M 3-15	6720 \pm 660	6530 \pm 910	0.049 \pm 0.024	1.792 \pm 0.504	2	[80]
Hen 2-86	7060 \pm 160	6890 \pm 220	0.039 \pm 0.008	1.321 \pm 0.116	7	[80]
M 2-31	7900 \pm 530	7680 \pm 660	0.063 \pm 0.018	1.091 \pm 0.260	4	[82]
NGC 5189	9370 \pm 780	9300 \pm 960	0.065 \pm 0.028	0.632 \pm 0.152	5	[80]
M 1-60	7010 \pm 250	6770 \pm 360	0.056 \pm 0.010	1.704 \pm 0.247	4	[82]
Hen 2-73	8770 \pm 610	8570 \pm 800	0.094 \pm 0.022	0.998 \pm 0.228	4	[82]
IC 4776	8390 \pm 120	8280 \pm 150	0.048 \pm 0.007	0.733 \pm 0.034	7	[84]
M 1-25	6640 \pm 340	6450 \pm 460	0.037 \pm 0.013	0.994 \pm 0.213	4	[80]
M 1-33	6780 \pm 210	6460 \pm 300	0.067 \pm 0.009	1.931 \pm 0.249	4	[82]
M 2-36	5450 \pm 70	4770 \pm 140	0.092 \pm 0.004	4.826 \pm 0.374	8	[85]
Abell 46	4240 \pm 60	320 \pm 370	0.279 \pm 0.008	11.149 \pm 1.056	6	[52]

Table A8 Ionic abundances of the H II regions and other nebulae.

Region	12+log(O ⁺ /H ⁺) CELs	12+log(O ²⁺ /H ⁺) CELs $t^2(O^{2+})=0$	12+log(O ²⁺ /H ⁺) RLs	Ref.
Extragalactic H II regions				
NGC 5461	7.78 ^{+0.08} _{-0.06}	8.29 ± 0.05	8.46 ^{+0.14} _{-0.13}	[62]
NGC 588	7.40 ^{+0.27} _{-0.11}	8.11 ^{+0.09} _{-0.06}	8.33 ± 0.08	[63]
NGC 595	8.29 ^{+0.05} _{-0.04}	8.02 ^{+0.14} _{-0.05}	8.34 ^{+0.08} _{-0.09}	[62]
K 932	7.87 ^{+0.05} _{-0.03}	8.30 ± 0.03	8.50 ± 0.07	[62]
IC 132	7.17 ^{+0.21} _{-0.14}	8.24 ^{+0.09} _{-0.06}	8.38 ± 0.10	[63]
N 11B	7.99 ^{+0.03} _{-0.04}	8.17 ^{+0.03} _{-0.01}	8.37 ± 0.03	[38]
NGC 5471	7.17 ^{+0.07} _{-0.06}	7.93 ^{+0.02} _{-0.01}	8.05 ± 0.15	[64]
N 66A	7.49 ^{+0.06} _{-0.04}	7.84 ± 0.02	7.99 ± 0.05	[38]
NGC 604	7.92 ± 0.06	8.23 ± 0.04	8.43 ± 0.07	[62]
NGC 6822	7.37 ^{+0.36} _{-0.16}	8.08 ^{+0.03} _{-0.02}	8.31 ^{+0.08} _{-0.07}	[65]
UV-1	7.80 ^{+0.14} _{-0.09}	8.09 ± 0.02	8.50 ^{+0.13} _{-0.14}	[66]
NGC 5408	7.29 ^{+0.14} _{-0.12}	7.70 ± 0.03	8.18 ± 0.10	[65]
NGC 1714	7.65 ^{+0.13} _{-0.08}	8.27 ^{+0.03} _{-0.05}	8.45 ± 0.07	[38]
N 81	7.30 ^{+0.04} _{-0.03}	7.90 ^{+0.03} _{-0.02}	8.22 ± 0.03	[38]
IC 2111	8.05 ^{+0.08} _{-0.06}	8.18 ± 0.04	8.34 ^{+0.09} _{-0.10}	[38]
NGC 2363	6.57 ^{+0.12} _{-0.13}	7.69 ^{+0.02} _{-0.03}	8.02 ^{+0.11} _{-0.10}	[62]
30Dor	7.62 ± 0.05	8.27 ± 0.01	8.42 ± 0.05	[67]
N 44C	7.30 ± 0.05	8.23 ± 0.02	8.56 ^{+0.04} _{-0.03}	[38]
HII-2	7.66 ^{+0.11} _{-0.10}	8.06 ± 0.02	8.57 ^{+0.15} _{-0.14}	[66]
NGC 5455	7.74 ± 0.03	8.18 ± 0.03	8.28 ^{+0.15} _{-0.14}	[64]
VS44	7.91 ^{+0.08} _{-0.06}	8.15 ^{+0.04} _{-0.06}	8.41 ± 0.15	[62]
N 88A	6.88 ± 0.07	8.00 ^{+0.02} _{-0.01}	8.18 ± 0.02	[38]
HII-1	7.59 ^{+0.09} _{-0.06}	8.07 ± 0.02	8.57 ± 0.16	[66]
Galactic ring nebulae				
NGC 7635A2	7.93 ^{+0.31} _{-0.11}	8.24 ^{+0.11} _{-0.08}	8.82 ± 0.13	[19]
NGC 7635A3	8.06 ^{+0.16} _{-0.07}	8.31 ^{+0.18} _{-0.10}	8.73 ± 0.11	[19]
NGC 7635A4	8.16 ^{+0.03} _{-0.05}	7.60 ^{+0.10} _{-0.08}	7.95 ± 0.11	[19]
NGC 6888A2	8.33 ± 0.04	7.52 ± 0.03	9.23 ± 0.09	[19]
NGC 6888A3	8.13 ± 0.06	7.69 ^{+0.15} _{-0.09}	8.86 ± 0.10	[19]
NGC 6888A4	7.47 ^{+0.06} _{-0.05}	7.95 ± 0.13	8.64 ^{+0.12} _{-0.13}	[19]
NGC 6888A5	7.49 ± 0.06	7.97 ^{+0.09} _{-0.07}	8.74 ^{+0.12} _{-0.11}	[19]
NGC 6888A6	7.57 ^{+0.05} _{-0.06}	7.98 ^{+0.17} _{-0.11}	8.56 ± 0.09	[19]

Table A8 Continued.

Region	12+log(O ⁺ /H ⁺) CELs	12+log(O ²⁺ /H ⁺) CELs $t^2(\text{O}^{2+})=0$	12+log(O ²⁺ /H ⁺) RLs	Ref.
Galactic H II regions				
NGC 3603	7.36 ^{+0.13} _{-0.09}	8.43 ^{+0.02} _{-0.03}	8.74 ± 0.11	[43]
M 42-P1	7.81 ^{+0.10} _{-0.07}	8.39 ± 0.02	8.55 ± 0.05	[72]
M 42-2	7.74 ^{+0.07} _{-0.05}	8.36 ± 0.02	8.61 ^{+0.02} _{-0.01}	[73]
Sh 2-100	7.76 ^{+0.11} _{-0.06}	8.38 ± 0.02	8.59 ± 0.08	[74]
M 42-3	7.75 ^{+0.07} _{-0.06}	8.36 ^{+0.01} _{-0.02}	8.55 ± 0.03	[75]
M 42-1	7.87 ± 0.06	8.33 ^{+0.02} _{-0.01}	8.49 ± 0.03	[75]
Sh 2-311	8.30 ± 0.04	7.82 ± 0.02	8.05 ^{+0.14} _{-0.15}	[76]
M 16	8.47 ^{+0.06} _{-0.05}	7.92 ^{+0.04} _{-0.03}	8.31 ^{+0.10} _{-0.11}	[43]
M 42-bar	8.39 ± 0.04	8.04 ± 0.02	8.23 ± 0.06	[72]
M 42-1	8.14 ^{+0.03} _{-0.04}	7.96 ± 0.01	8.17 ± 0.03	[46]
NGC 3576	8.06 ^{+0.08} _{-0.05}	8.36 ± 0.01	8.66 ± 0.03	[77]
M 42	7.81 ^{+0.07} _{-0.06}	8.40 ± 0.01	8.64 ± 0.03	[42]
M 17	7.82 ^{+0.06} _{-0.04}	8.45 ± 0.02	8.69 ^{+0.08} _{-0.07}	[44]
M 8	8.34 ^{+0.04} _{-0.03}	7.88 ^{+0.02} _{-0.03}	8.24 ± 0.06	[44]
M 42-4	7.81 ^{+0.06} _{-0.05}	8.36 ± 0.02	8.54 ± 0.02	[75]
M 42-3	7.68 ± 0.05	8.38 ^{+0.01} _{-0.02}	8.63 ± 0.02	[73]
Sh 2-288	8.22 ^{+0.08} _{-0.07}	7.72 ^{+0.11} _{-0.08}	8.11 ^{+0.17} _{-0.15}	[74]
M 42	7.94 ± 0.07	8.35 ^{+0.05} _{-0.04}	8.51 ± 0.07	[78]
M 42-2	8.17 ^{+0.03} _{-0.04}	8.03 ^{+0.02} _{-0.01}	8.40 ± 0.04	[46]
M 42-2	7.82 ± 0.05	8.36 ± 0.02	8.52 ± 0.01	[75]
Extragalactic H II regions from the literature				
NGC 456a-1	7.65 ± 0.06	7.84 ± 0.01	8.22 ± 0.10	[68]
NGC 456a-2	7.53 ^{+0.25} _{-0.10}	7.93 ± 0.01	8.34 ^{+0.15} _{-0.14}	[68]
NGC 6822V	6.91 ^{+0.25} _{-0.14}	8.06 ^{+0.03} _{-0.02}	8.27 ^{+0.13} _{-0.14}	[69]
NGC 5253C1	7.34 ± 0.02	8.08 ± 0.01	8.11 ± 0.07	[68]
Mrk1259	8.36 ^{+0.08} _{-0.07}	7.75 ^{+0.06} _{-0.05}	8.97 ± 0.13	[68]
NGC 5253C2	7.56 ^{+0.07} _{-0.05}	8.17 ± 0.01	8.31 ± 0.09	[68]
NGC 5253P2	7.42 ^{+0.04} _{-0.03}	8.07 ± 0.01	8.35 ± 0.10	[68]
NGC 346	7.32 ^{+0.14} _{-0.11}	7.93 ± 0.01	8.28 ^{+0.08} _{-0.07}	[70]
NGC 456-2	7.54 ^{+0.15} _{-0.11}	7.88 ^{+0.02} _{-0.01}	8.16 ^{+0.12} _{-0.13}	[71]

Table A8 Continued.

Region	12+log(O ⁺ /H ⁺) CELs	12+log(O ²⁺ /H ⁺) CELs $t^2(\text{O}^{2+})=0$	12+log(O ²⁺ /H ⁺) RLs	Ref.
Galactic planetary nebulae				
NGC 2440	7.41 ^{+0.09} _{-0.06}	8.22 ^{+0.02} _{-0.03}	8.50 ^{+0.03} _{-0.04}	[79]
Hb 4	7.33 ^{+0.19} _{-0.10}	8.59 ± 0.05	9.20 ± 0.07	[80]
NGC 5315	7.83 ^{+0.32} _{-0.23}	8.69 ^{+0.07} _{-0.05}	8.95 ± 0.05	[81]
M 1-31	7.68 ^{+0.13} _{-0.11}	8.74 ^{+0.05} _{-0.04}	9.06 ± 0.10	[82]
Cn 1-5	8.10 ^{+0.13} _{-0.07}	8.69 ± 0.04	9.00 ^{+0.09} _{-0.10}	[80]
H 1-40	7.02 ^{+0.13} _{-0.10}	8.49 ^{+0.05} _{-0.04}	8.96 ± 0.17	[82]
H 1-50	7.38 ^{+0.10} _{-0.07}	8.60 ^{+0.03} _{-0.04}	9.04 ± 0.07	[82]
Hen 2158	7.88 ± 0.07	8.35 ± 0.03	8.57 ^{+0.15} _{-0.16}	[82]
IC 418	8.37 ^{+0.08} _{-0.06}	8.08 ± 0.02	8.26 ^{+0.05} _{-0.04}	[83]
PC 14	7.35 ^{+0.11} _{-0.08}	8.73 ^{+0.04} _{-0.03}	9.07 ^{+0.08} _{-0.09}	[80]
M 1-32	8.25 ^{+0.17} _{-0.11}	8.28 ^{+0.05} _{-0.04}	8.78 ^{+0.07} _{-0.06}	[80]
M 1-61	7.15 ^{+0.24} _{-0.14}	8.63 ^{+0.06} _{-0.05}	8.93 ± 0.07	[80]
Ou5	6.27 ^{+0.48} _{-0.17}	7.98 ^{+0.03} _{-0.04}	10.06 ^{+0.09} _{-0.08}	[52]
NGC 6369	6.91 ^{+0.10} _{-0.07}	8.50 ^{+0.05} _{-0.03}	8.73 ± 0.09	[80]
Pe 1-1	7.48 ^{+0.25} _{-0.18}	8.53 ^{+0.05} _{-0.04}	8.85 ± 0.10	[80]
IC 2501	7.50 ^{+0.04} _{-0.05}	8.58 ± 0.02	8.60 ± 0.03	[79]
M 1-30	8.42 ^{+0.14} _{-0.08}	8.50 ^{+0.06} _{-0.04}	8.96 ^{+0.04} _{-0.05}	[80]
IC 4191	7.30 ± 0.08	8.79 ^{+0.03} _{-0.02}	9.10 ± 0.02	[79]
Hen 2-96	7.43 ^{+0.16} _{-0.14}	8.63 ^{+0.05} _{-0.04}	8.83 ± 0.10	[82]
M 3-15	6.88 ^{+0.16} _{-0.08}	8.78 ± 0.05	9.19 ^{+0.12} _{-0.11}	[80]
Hen 2-86	7.42 ^{+0.30} _{-0.21}	8.76 ^{+0.05} _{-0.04}	9.07 ± 0.04	[80]
M 2-31	7.43 ± 0.08	8.60 ± 0.05	8.97 ± 0.10	[82]
NGC 5189	8.13 ^{+0.11} _{-0.07}	8.43 ± 0.04	8.70 ^{+0.11} _{-0.10}	[80]
M 1-60	7.74 ^{+0.21} _{-0.13}	8.76 ^{+0.05} _{-0.04}	9.17 ^{+0.06} _{-0.07}	[82]
Hen 2-73	7.54 ^{+0.11} _{-0.10}	8.51 ± 0.05	8.93 ± 0.10	[82]
IC 4776	7.76 ^{+0.45} _{-0.14}	8.53 ± 0.03	8.81 ± 0.02	[84]
M 1-25	8.29 ^{+0.10} _{-0.09}	8.62 ± 0.05	8.94 ± 0.09	[80]
M 1-33	7.68 ^{+0.08} _{-0.05}	8.72 ± 0.04	9.22 ± 0.06	[82]
M 2-36	6.95 ^{+0.05} _{-0.04}	8.72 ^{+0.03} _{-0.02}	9.61 ± 0.03	[85]
Abell 46	6.25 ^{+1.05} _{-0.19}	7.75 ^{+0.03} _{-0.02}	9.95 ± 0.04	[52]